

Short Hard Gamma Ray Bursts And Their Afterglows

Shlomo Dado¹ and Arnon Dar²

ABSTRACT

Long duration gamma ray bursts (GRBs) and X-ray flashes (XRFs) are produced by highly-relativistic jets ejected in core-collapse supernova explosions. The origin of short hard gamma-ray bursts (SHBs) has not been established. They may be produced by highly relativistic jets ejected in various processes: mergers of compact stellar objects; large-mass accretion episodes onto compact stars in close binaries or onto intermediate-mass black holes in dense stellar regions; phase transition of compact stars. Natural environments of such events are the dense cores of globular clusters, superstar clusters and young supernova remnants. We have used the cannonball model of GRBs to analyze all Swift SHBs with a well-sampled X-ray afterglow. We show that their prompt gamma-ray emission can be explained by inverse Compton scattering (ICS) of the progenitor's glory light, and their extended soft emission component by ICS of high density light or synchrotron radiation (SR) in a high density interstellar medium within the cluster. The mechanism generating the afterglow is synchrotron radiation outside the cluster. No associated supernova could be detected in the low luminosity nearby GRBs 060614 and 060505. We interpret them as SHBs seen relatively far off axis.

1. Introduction

Gamma ray bursts (GRBs) have been traditionally classified into short hard bursts (SHBs) and long soft bursts. Their distribution as a function of duration is bimodal with a minimum around two seconds (Mazets et al. 1981; Norris et al. 1984, Kouveliotou et al. 1993). The γ -rays of short bursts are typically harder than those of long bursts, thus

¹dado@phep3.technion.ac.il

Physics Department and Space Research Institute, Technion, Haifa 32000, Israel

²arnon@physics.technion.ac.il, dar@cern.ch

Physics Department and Space Research Institute, Technion, Haifa 32000, Israel
Theory Unit, CERN, 1211 Geneva 23, Switzerland

their acronym, SHBs, but their fluence is much smaller. The short hard bursts consist of a single or a complex of peaks with a total duration typically less than 2 seconds and peak widths which range between a few ms and a fraction of a second. The lag-time between their emission in soft and hard energy band is much smaller than that in long GRBs and X-ray flashes (XRFs). We shall refer to the ensemble of long GRBs and XRFs as LGRBs.

A true breakthrough in the observations of SHBs came with the launch of Swift in November 2004. Since its launch Swift has detected over 30 SHBs with X-ray and UVO afterglows, and triggered follow-up ground-based observations that for most SHBs succeeded in identifying their host galaxy and measuring its redshift. Swift has also discovered that, in more than 25% of these cases, perhaps in all, the SHB was followed by an extended soft emission component (ESEC), a spectrally softer component lasting tens of seconds (for recent reviews see Nakar 2007, Kann et al. 2008). The fluence of SHBs is typically much smaller than that of GRBs. The fluence of their ESEC is usually comparable to or smaller than that of the SHB. The ESECs end with a fast-decay phase, followed by an afterglow with a canonical time-dependence, similar to the one observed in a large fraction of LGRBs (Nousek et al. 2006). LGRBs are located near the center of their hosts, which are all late-type galaxies (Covino et al. 2006). Contrariwise, SHBs have an heterogeneous population of hosts, and take place both in elliptical galaxies (e.g., SHBs 050709 and 050724, Gehrels et al. 2005, Berger et al. 2005) and spiral galaxies (e.g., SHB 051221A, Soderberg et al. 2006c). Generally, the SHBs with an ESEC are centrally located, while those with no detectable ESEC are found at very large distances from their host’s center (Troja et al. 2008). There is also a clear trend of their afterglow to be fainter for larger offsets (Kann et al. 2008).

Observations indicate that LGRBs are mainly produced by core-collapse supernovae (SNe) of type Ib/c. A GRB-SN association was discussed long ago (Colgate 1968, Dar et al. 1992) but was dismissed by Woosley (1993) who suggested that only ‘failed supernovae’ produce GRBs. Following the discovery by Galama et al. (1998) of SN1998bw in the error box of GRB980425, Wang & Wheeler (1998), Dar & Plaga (1999) and Dar & De Rújula (2000) suggested that perhaps most core collapse SNe produce LGRBs. This was later advocated as an observed fact, based on a comprehensive analysis of optical afterglows within the cannonball (CB) model of LGRBs (Dado, Dar & De Rújula 2002,2003 hereafter DDD2002,DDD2003, Dar & De Rújula 2004 hereafter DD2004, and references therein) and on empirical grounds by Zeh, Klose & Hartmann (2004). General acceptance of the GRB-SN association waited until the spectroscopic discovery of an SN2003dh coincident with GRB030329 (Hjorth et al. 2003, Stanek et al. 2003) and b additional discoveries of spectroscopically proven GRB-SN associations such as GRB030213/SN2003lw (Malesani et al. 2003), GRB021211/SN2002lt (Della Valle et al. 2003), XRF060218/SN2006aj (Campana et al. 2006a, Pian et al. 2006, Mazzali et al. 2006) and XRF080109/SN2008D (Malesani et

al. 2008, Modjaz et al. 2008).

In contrast, SHBs do not seem to be associated with any known type of supernova (e.g., Hjorth et al. 2005b). The identity of their progenitors is not established, except that giant flares from soft gamma ray repeaters (SGRs) that look like SHBs, may account for most of the observed SHBs in nearby (redshift $z \lesssim 0.01$) galaxies (Dar 2005, Hurley et al. 2005). The extremely bright SHBs 051103 and 070201 observed by Konus-Wind could have been such events in the nearby galaxies M81/M82 and M31 (Ofek et al. 2006, Frederiks et al. 2007). But hyperflares from SGRs cannot account for the bulk of the much more distant ones, $z \gg 0.01$, unless they are highly collimated or much more energetic but less frequent.

Although the observational data on cosmological SHBs and their afterglows did not pin down their progenitors, they do provide useful clues to their progenitors, production mechanism, and production sites. Their extremely short durations and large equivalent isotropic gamma ray energies, and the absence of self absorption features in their γ -ray spectra suggest that they are produced by highly relativistic jets ejected in violent processes involving compact stars (Shaviv & Dar 1995a) such as:

- Neutron stars merger and neutron star - black hole merger in compact binaries (Blinnikov et al. 1984, Paczynski 1986, Goodman, Dar & Nussinov 1987, Eichler et al. 1989).
- Collapse of compact stars (neutron stars, hyper stars, quark stars) to a more compact star due to mass accretion, and/or loss of angular momentum and/or cooling by radiation (Dar 1998a,1999, Dar & De Rújula 2000, Dar 2006).
- Phase transition in compact stars, such as neutron-stars, hyper-stars and quark stars (Dar 1999, Dar & De Rújula 2000, Dar 2006).
- Accretion episodes in microblazars (Dar 1998b,1999) and on intermediate mass black holes in dense stellar regions.

The natural environment of these progenitors are super dense stellar regions such as collapsed cores of globular clusters (GCs) and young centrally-condensed super-star cluster (SSC) (Shaviv & Dar 1995b) whose stellar densities and total luminosities seem to be correlated with their distance from the center of their host galaxy. If the ESEC is produced by ICS of ambient light in globular clusters with a low density interstellar medium (ISM) or by synchrotron radiation (SR) in super-star clusters with a very large ISM density, it may explain the observations that SHBs with an ESEC are centrally located, while those with no detectable ESEC are found at very large distances from their host's center (Troja et al. 2008).

The spectra and pulse-shapes of SHBs measured by the γ -ray telescopes on board satellites, except for being harder and shorter, are very similar to those measured by the same satellites in LGRBs (Nakar 2006, Kann et al. 2008). In particular, the X-ray light curves of SHBs, which were well sampled with the Swift Burst Alert Telescope (BAT) and X-ray Telescope (XRT) show the same canonical behaviour seen in many LGRBs (Nousek et al. 2006, O’Brien et al. 2006): An early rapid temporal decay of the prompt emission during which the spectrum softens at a very fast rate. This rapid decay phase ends within a few hundred seconds when it is taken over by a plateau with a much harder power-law spectrum, typically lasting thousands to tens of thousands of seconds. Within a time of order of one day, the plateau steepens into a power-law decay, which lasts until the X-ray AG becomes too dim to be detected. Often, X-ray flares, not coinciding with any detectable γ -ray activity, are superimposed on the X-ray light curve during the fast-decaying phase and even later. These similarities with long GRBs suggest that the initial burst and the afterglow in both SHBs and LGRBs are produced by the same radiation mechanisms: inverse Compton scattering (ICS) of glory light and synchrotron radiation (SR) from decelerating CBs.

The CB model has been successful in predicting/accommodating the observed properties of the prompt radiation of LGRBs (Dar & De Rújula 2004 - hereafter DD2004) and their afterglows (Dado, Dar & De Rújula 2002, 2003, 2007b, 2008a,b - hereafter DDD2002, DDD2003, DDD2007b, DDD2008a,b,c). Because of the above similarities between LGRBs and SHBs, the CB model may also reproduce correctly the main observed properties of SHBs, after only simple adjustments. Indeed, in this paper we show that using only general properties of the putative SHB progenitors and their natural environments, the CB model with the same two basic radiation mechanisms, ICS of ambient light, which dominates the prompt emission, and synchrotron radiation which dominates the afterglow emission, provides also a simple and successful description of the observed properties of SHBs and their afterglows. Moreover, a few nearby LGRBs without a detectable supernova, such as GRB 060614, which were interpreted as belonging to a new class of LGRBs (e.g., Gal-Yam et al. 2006b, Gehrels et al. 2006, Della Valle et al. 2006) can be interpreted as SHBs seen far off-axis.

2. Summary of the underlying assumptions

2.1. The progenitors of GRBs and their environments

We have no novel suggestions regarding either the putative progenitors of cosmological SHBs or the ejection mechanism and the properties of their highly relativistic jets. As listed in the introduction, most conventionally, the progenitors may be the merger of a neu-

tron star with another one or with a black hole, or large accretion episodes in microblazars (microquasars with their jets pointing accurately to us) or intermediate mass black holes. Accretion, cooling or angular momentum loss may result in abrupt transitions of neutron stars to more compact objects (strange stars, quark stars or stellar black holes). All these phenomena are natural candidates for SHB progenitors. The above putative progenitors meet the energy-budget requirements, even if the radiation of SHBs is not very highly collimated. The estimated merger rate of neutron stars is sufficient only if SHBs are not narrowly collimated. If they are, as in the CB model, some of the other mechanisms we cited must also be operative. Indeed, low-luminosity LGRBs detected by INTEGRAL led to the conclusion (Foley et al. 2008) that the rate of LGRBs with inferred low luminosity is $\gtrsim 25\%$ of that of Type Ib/c supernovae¹. Since BATSE observed an SHB rate nearly 1/3 the rate of LGRBs, the rate of SHBs implied by the INTEGRAL observations must also be comparable to the rate of SNe of type Ib/c. Such a rate is a considerable fraction of the birth rate of neutron stars. It is much larger than the merger rate of neutron stars in close binaries. It favours other alternative sources of SHBs such as a phase transition in neutron stars or accretion episodes on stellar mass and intermediate mass, black holes.

The putative progenitors of SHBs are mostly located in the cores of globular clusters and the central region of superstar clusters. We shall assume that SHBs are produced in such an environment.

2.2. The Radiation mechanisms

We shall assume that similar to LGRBs, the two dominant radiation mechanism in SHBs are ICS and SR. The ICS of glory light produced by a stellar companion or by an accretion disk, by electrons comoving with the CBS, dominates the prompt emission, while SR from the decelerating CBs in the ISM or the intergalactic medium (IGM) dominates the afterglow emissions.

We shall also assume that ICS of ambient light in globular clusters of low density ISM, or SR from the decelerating CBs in the high density ISM of superstar clusters produces the ESEC.

¹Such a fraction is larger by a factor $\sim 10^2-10^3$ than that of previous estimates (e.g., Gal-Yam et al. 2006a and Soderberg et al. 2006b), which relied on the validity of uncertain fireball model relations.

2.3. The main parameters

The launching of highly relativistic and narrowly collimated jets in mass accretion episodes, merger or phase transitions is not sufficiently understood to predict the chaotic timing of CB emissions, nor the number, N_{CB} , of dominant CBs in a particular jet, nor the baryon number, N_B , nor the initial Lorentz factor, γ_0 , of observable CBs. But once the typical values of these parameters are inferred from the data, all properties of LGRBs and SHBs can be understood in simple terms. This also requires a number of items of information independent of the model itself. They are the angle between a CB jet and the observer, the properties of the ambient light a CB encounters in its flight, and of the density of the interstellar medium (ISM) or intergalactic medium (IGM) which CBs pierce through. Naturally, the cosmological redshift, z , and the absorption or attenuation of light of various frequencies along the line of sight play their usual roles, with the exception, in comparison with other models, that the line of sight to a CB moves significantly (and hyper-luminally) during the observation time. The standard cosmological model with $\Omega = 1$, $\Omega_M = 0.27$, $\Omega_\Lambda = 0.73$ and $H_0 = 71 \text{ km s}^{-1}, \text{ Mpc}^{-1}$ is assumed throughout this paper.

2.4. The opening angle of a jet of CBs and the typical observers' angle

We hypothesize that a CB initially expands in its rest system at a speed comparable to the speed of sound in a relativistic plasma, $v \equiv \beta_s c / \sqrt{3}$ with $\beta_s \lesssim 1$. A CB's initial radius must be of the order of the size of the progenitor compact object or its accretion disk, and rapidly becomes negligible as the CB expands. Thus, a CB traces a cone in space of initial opening angle $\theta_{CB} = \beta_s / \sqrt{3} \gamma_0$. The characteristic opening angle of the emitted radiation is $1/\gamma_0$, much larger than θ_{CB} , so that the jet opening is not a concept that plays a very major role. In the AG phase, the effect of the deceleration of CBs in the ISM becomes important, and the radiation is spread over an angle $1/\gamma(t)$.

In the CB model, the Doppler factor, $\delta(t)$, relating times, energies and fluxes in a CB's rest system to those in the observer's system plays a major role in the understanding GRBs. Its form in terms of θ and the time-dependent Lorentz factor, $\gamma(t)$, of a CB, is:

$$\delta(t) = \frac{1}{\gamma(t) (1 - \beta(t) \cos \theta)} \approx \frac{2\gamma(t)}{1 + [\gamma(t) \theta]^2}, \quad (1)$$

where the approximation is excellent for $\gamma \gg 1$ and $\theta \ll 1$. Doppler boosting and relativistic beaming enhances the observed energy flux from a CB by a factor δ^3 , making the observations of GRBs increasingly improbable to observe GRBs at angles $\theta > 1/\gamma$. The angular phase space being $d\Omega \propto \theta d\theta$, the most probable angle of observation is $\approx 1/\gamma$.

3. The prompt emission

3.1. The spectrum of ICS pulses

We contend that the prompt γ and X-rays of an SHB's pulse are made similar to those in LGRBs, i.e., by ICS of glory light by the electrons contained within a CB. For LGRBs the glory light is the early flash of the SN explosion, scattered away from the radial direction by the nearby circumburst material ejected by pre-SN ejecta. For the prompt signal of SHBs, the glory light may be the light emitted by a companion star or a transient accretion disk and scattered by their winds. During the initial phase of γ -ray emission in a SHB, the Lorentz factor γ of a CB stays put at its initial value γ_0 , for the deceleration induced by the collisions with the ISM has not yet had a significant effect. The electrons comoving with the CB scatter the photons of the glory around the progenitor, which has a thin thermal-bremsstrahlung spectrum,

$$\epsilon \frac{dn_\gamma}{d\epsilon} \sim \left(\frac{\epsilon}{\epsilon_g} \right)^{-\beta_g} e^{-\epsilon/\epsilon_g}, \quad (2)$$

with a spectral index $\beta_g \sim 0$ (photon spectral index $\Gamma = \beta_g + 1 \sim 1$) and a typical (pseudo)-temperature, $\epsilon_g \sim 2$ eV, for a glory produced by stellar light. The observed energy of a glory photon, which suffered an inverse Compton scattering by an electron comoving with a CB at redshift z , is then given by,

$$E = \frac{\gamma_0 \delta_0 \epsilon}{(1+z)} (1 + \cos \theta_{in}), \quad (3)$$

where θ_{in} is the angle of incidence of the initial photon onto the CB, in the SN rest system.

The density of the glory photons seen by a CB is given roughly by, $n_g(r) \sim n_g(0) r_g^2 / (r^2 + r_g^2)$. At an early time, $r \approx c \gamma_0 \delta_0 t / (1+z)$. Consequently, $n_g(t) \sim n_g(0) \Delta t^2 / (t^2 + \Delta t^2)$, where $\Delta t = (1+z) r_g / c \gamma_0 \delta_0$. The factor $1 + \cos \theta_{in}$ in Eq. (3) must roughly average zero near the center of the glory where the photon distribution is semi isotropic and tends to $1/r^2 \sim 1/t^2$ as the CB moves away. This behaviour is described approximately by $\langle 1 + \cos \theta_{in} \rangle \approx 1 - t / \sqrt{t^2 + \Delta t^2}$ and then the predicted time-dependent spectrum of the SHB pulse, produced by ICS of the glory photons and observed at an angle θ , is given by (DD2004):

$$E \frac{dN_\gamma}{dE} \sim \left(\frac{E}{E_p(t)} \right)^{-\beta_g} e^{-E/E_p(t)} + b(1 - e^{-E/E_p(t)}) \left(\frac{E}{E_p(t)} \right)^{-p/2}, \quad (4)$$

where,

$$\begin{aligned} E_p(t) &\simeq E_p(0) \left[1 - \frac{t}{\sqrt{t^2 + \Delta t^2}} \right], \\ E_p(0) &= \frac{\gamma_0 \delta_0}{1+z} \epsilon_g. \end{aligned} \quad (5)$$

The first term, with $\beta_g \sim 0$, is the result of Compton scattering by the bulk of the CB’s electrons, which are comoving with it. The second term in Eq. (4) is induced by a very small fraction of ‘knocked on’ and Fermi accelerated electrons, whose initial spectrum (before Compton and synchrotron cooling) is $dN_e/dE \propto E^{-p}$, with $p \approx 2.2$. For $b = O(1)$, the predicted spectrum, Eq. 4, bears a striking resemblance to the empirical Band function (Band et al. 1993) traditionally used to model the energy spectra of GRBs. GRBs which are well fit by the Band function are also well fit by Eq. (4), but GRBs where the spectral measurements extended over a much wider energy range than that of BATSE and Swift/BAT, were better fit by Eq. 4 (e.g., Wigger et al. 2008).

For many Swift SHBs the spectral observations do not extend to energies larger than $E_p(0)$, or the value of b in Eq. (4) is relatively small because of the low-density environment of the SHB, so that the first term of the equation,

$$E \frac{dN_\gamma}{dE} \sim \left(\frac{E}{E_p(t)} \right)^{-\beta_g} e^{-E/E_p(t)}. \quad (6)$$

with $\beta_g \simeq 0$ ($\Gamma = 1 - \beta_g \simeq 1$) provides a very good approximation, and will be used in this paper. This term coincides with the ‘cut-off power-law’ spectrum which has been used to model the time integrated spectra of many LGRBs and SHBs. The resulting values of Γ that are reported in Table I for time integrated spectra, are all consistent within the observational uncertainties with the ICS expected value, $\Gamma = 1$.

3.2. The light curve of the prompt ICS pulses

After its launch, the fast expanding CB propagates in the progenitor’s glory and wind on its way to the ISM. Its cross section increases, while both its density and opacity, as well as those of the wind, decrease. The pressure of the incoming particles and radiation on its front surface may distort its shape to look more like a disk. Let t be the time after launch of a CB in the rest frame of the progenitor. Approximating the CB geometry by a cylindrical slab of radius R and neglecting the spread in arrival times of scattered glory photons in the CB that entered it simultaneously, the rate of scattered glory photons is given by,

$$\frac{dN_\gamma}{dt} = \pi R^2(t) c n_g(t) \int dt' c \sigma_T n(t') e^{-\int_t^{t'} \sigma_T n(t'') c dt''}. \quad (7)$$

The integration yields

$$\frac{dN_\gamma}{dt} = c n_g(t) \pi R^2(t) [1 - e^{-\sigma_T N(t)}], \quad (8)$$

where $N(t)$ is the effective column density of the expanding CB encountered by a photon which begins crossing it at a time t .

If t denotes the time of arrival of photons seen by a distant observer, it is related to the time t_r in the progenitor’s rest frame via $dt = (1 + z) dt_r / \gamma_0 \delta_0$. The relativistic motion of the CB that boosts the energy of the ICS photons, also collimates them by a factor $d\cos\theta/d\cos\theta_r = \delta_0^2$. Thus, the pulse produced by a CB at redshift z and luminosity distance d_L is described approximately by,

$$E \frac{d^2 N_\gamma}{dt dE} \approx \frac{c n_g(t) (1 + z) \gamma_0 \delta_0^3}{4 \pi d_L^2} e^{-\tau_w(t)} \pi R^2(t) [1 - e^{-4 R_{tr}^2 / 3 R^2(t)}] E \frac{dN_\gamma}{dE}, \quad (9)$$

where $\tau_w = \sigma_w \int_r n(r) dr \sim a/t$ is the radiative opacity of the wind, and $E dN_\gamma/dE$ is given by Eq. (4). A wind’s density-profile, $n(r) = n_0 r_0^2 / r^2$, yields, $a(E) = \sigma_w n_0 r_0^2 (1 + z) / c \gamma_0 \delta_0$. At sufficiently high energies the wind’s opacity is mainly due to Compton scattering, i.e., $\sigma_w \approx \sigma_T$, where σ_T is the Thomson cross section. At X-ray energies it is mainly due to bound-free and bound-bound transitions, and at energies below the threshold for atomic photo excitation it is dominated by free-free transitions and dust scattering.

The initial rapid expansion of a CB slows down as it propagates through the wind and scatters its particles (DDD2002, DD2004). This expansion can be described roughly by, $R^2 \approx R_{cb}^2 t^2 / (t^2 + t_{exp}^2)$, where R_{cb} is the asymptotic radius of the CB. Since $t_{tr} \ll t_{exp}$ (DD2004), Eq. (9) can be well approximated by,

$$E \frac{d^2 N_\gamma}{dt dE} \propto \frac{\Delta t^2 t^2 e^{-a/t}}{(t^2 + \Delta t^2)(t^2 + t_{tr}^2)} E \frac{dN_\gamma}{dE}, \quad (10)$$

For nearly transparent winds ($a \rightarrow 0$) and $t_{tr} \approx \Delta t$, Eq. (10) has an approximate shape,

$$E \frac{d^2 N_\gamma}{dt dE} \propto \frac{\Delta t^2 t^2}{(t^2 + \Delta t^2)^2} E \frac{dN_\gamma}{dE}. \quad (11)$$

Except for very early times, this shape is almost identical to that of the ‘Master’ formula advocated in (DD2004) for the prompt ICS pulses of GRBs and XRFs, which was shown to well describe the prompt emission pulses of LGRBs (e.g., DDD2007b, DDD2008a,b), including the rapid decay of the prompt emission and its a fast spectral softening (DDD2008a).

The observed light curve (energy flux density) of a multi-pulse SHB dominated by ICS is given by,

$$F_E \approx \sum_i A_i \Theta[t - t_i] \frac{\Delta t_i^2 (t - t_i)^2}{((t - t_i)^2 + \Delta t_i^2)^2} e^{-E/E_{p,i}(t-t_i)}. \quad (12)$$

where the index ‘i’ denotes the i-th ICS pulse produced by a CB launched at an observer time $t = t_i$, with a light curve given approximately by Eq. (11), and where,

$$A_i \approx \frac{c n_g(0) \pi R_{CB}^2 \gamma_0 \delta_0^3 (1 + z)}{4 \pi D_L^2}. \quad (13)$$

Thus, in the CB model each ICS pulse is effectively described by four parameters, t_i , A_i , Δt_i and $E_{p,i}(0)$, which are best fit to reproduce its observed light curve.

3.3. Effective spectral index and hardness ratio

The effective spectral index of unabsorbed ICS pulses in Eq. (6) is given by (DDD2008a),

$$\Gamma_i(E, t - t_i) = -E \frac{d \log F_E}{dE} = 1 + \beta_g + \frac{E}{E_{p,i}(t - t_i)}. \quad (14)$$

The hardness, defined as the ratio between the number of events in two energy bands, is generally reported, uncorrected for absorption, for the Swift 25-150 keV and 15-25 keV bands. It can be approximated by (DDD2008a),

$$\text{HR}_i(t) = B_i e^{-\Delta E/E_{p,i}(t-t_i)} \quad (15)$$

where ΔE is an effective interval between the bands.

3.4. The peak energy of a GRBs pulse

For $b \sim 0$ and $\beta_g \sim 0$, Eq. 4 yields a peak value of $E^2 dN/dE$ at $E = E_p(t)$. Observers usually report $E_p(t)$ at the peak's maximum, or its averaged value in a chosen time interval. For the approximate pulse shape given by Eq. 11, $E_p(t_{max}) \approx 0.29 E_p(0)$ while $E_p \approx 0.23$ over the FWHM of a pulse.

For LGRBs, Eqs. (5) give a good description of the observations, for $\epsilon_g \approx 2$ eV, $\gamma_0 \sim 10^3$, and $\delta_0 \sim 10^3$ corresponding to the expected $\theta \sim 1/\gamma_0$. As their name reflects, SHBs typically have a larger E_p than LGRBs. One reason is model-independent: SHBs are observed at smaller typical redshifts. In the CB model, according to Eqs. (5), larger values of $(1+z) E_p$ may be due to a larger value of the typical ϵ_g and/or γ_0 . The glory of LGRBs being the very early light of a core-collapse SN, there are observational reasons to adopt $\epsilon_g \approx 2$ eV. For SHBs the ambient light may be the light of a companion star, or of an accretion disk. In the first case, there is also reason to adopt $\epsilon_g \approx 2$ eV, which we will use for the sake of definiteness. The typical Lorentz and Doppler factors leading to the average value of $(1+z) E_p \sim 800$ keV for the well-measured cases in the table of SHB properties of Kann et al. (2008) are:

$$\gamma_0[\text{SHB}] \sim \delta_0[\text{SHB}] \sim 1400, \quad (16)$$

somewhat larger than the typical values, $\gamma_0 \sim \delta_0 \sim 10^3$ for LGRBs.

3.5. The width and time-lag of SHB pulses

The peak time of dN/dt for the pulse-shape given by Eq. (11) is around $t = \Delta t = t_{tr}$, where

$$t_{tr} \approx \frac{\sqrt{3}(1+z)}{\delta_0 \beta_s} \frac{R_{tr}}{c} \approx \frac{23 \text{ ms}}{\beta_s} \frac{10^3}{\delta_0} (1+z) \sqrt{\frac{N_B}{10^{48}}}. \quad (17)$$

The full width of dN/dt at half maximum is $\text{FWHM} \sim 2.38 t_{tr}$ and its rise-time from half maximum to peak value is $t_{rise} \sim 0.59 t_{tr}$ ($\text{FWHM} \sim 1.8 t_{tr}$ and $t_{rise} \sim 0.7 t_{tr}$ for the pulse shape used in DDD2004). The pulse-shape is energy-dependent because of the exponential factor in the pulse light curve,

$$E \frac{d^2 N}{dE} \propto e^{-E/E_p(t)} \rightarrow e^{-2Et^2/E_p(0)\Delta t^2}, \quad (18)$$

and the rise time, peak time and FWHM of the ICS pulse are energy-dependent and decrease with increasing energy. In the CB model, this explains the observed time-lag effect in LGRB pulses which decreases with increasing energy. As can be seen from Eq. (18), the time-lag is proportional to the width parameter, Δt , and decreases with increasing E_p , yielding a vanishingly small time-lag in SHBs with a very small width and a large E_p . For $t^2 \gg \Delta t^2$, the pulse has a shape,

$$\frac{d^2 N}{dt dE} \propto (Et^2)^{-1} e^{-2Et^2/E_p(0)\Delta t^2} = F(Et^2). \quad (19)$$

This ‘ Et^2 ’ law is a test of ICS on a glory’s light that is becoming more radially directed at increasing radii and times: $\langle 1 + \cos\theta_{in} \rangle \rightarrow r_g^2/2r^2 \sim \Delta t^2/2t^2$ in Eq. (11). This law, in its form as a correlation between the FWHM of collections of pulses and the energy interval at which they are measured ($\text{FWHM} \sim E^{-1/2}$) has been known for a long time (e.g., Ramirez-Ruiz & Fenimore et al. 2000). For well-measured single-pulse XRFs, Eq. (19) can be tested with precision, from X-ray to optical frequencies, both as an (E, t) correlation and as a spectral form (DDD2007b). One example is XRF 060218, specifically discussed in De Rújula (2008). For SHBs we do not have enough information to test Eq. (19) and its underlying assumption that the source of the ambient light is localized close to, or around, the engine.

The measured redshifts of SHBs are relatively small, averaging $\langle z \rangle \sim 0.5$ compared with those of LGRBs; $\langle z \rangle \sim 2$. The widths of their pulses have been studied in more detail than their rise times, and range from 5 to 300 ms, with a broad peak at 50 ms (Nakar 2007, Kann et al. 2008). These numbers correspond to full widths at quarter maximum, $\text{FWQM} \sim 3.5 t_{tr}$ for the pulse shapes. The typical values $\gamma_0 = \delta_0 = 1400$, $z = 0.5$, and $\Delta t = 10$ ms in the observer’s frame correspond to $r_g = c\gamma(t)\delta(t)\Delta t/(1+z) \approx 4 \times 10^{14}$ cm in the progenitor’s rest frame. Inverting Eq. (17) and using $\gamma_0 = \delta_0 = 1400$, we obtain $N_B[\text{SHBs}] \sim 10^{48}$ for $\text{FWQM} = 50$

ms and $\beta_S = 1/3$, respectively. This is smaller than the typical $N_b[\text{LGRBs}] \sim 10^{50}$ by two orders of magnitude, probably because core-collapse SNe have much more available mass for potential CB-generating accretion than any of the putative SHB progenitors.

3.6. The peak luminosity and isotropic energy of SHBs

Let L be the luminosity of the source (an accretion disk or a massive companion). For a transparent or semi-transparent distribution of circumburst material, it is approximately the glory's luminosity. The peak luminosity of a CB is at $t = t_{tr}$, the time it becomes of transparent, and it is given by (DD2004),

$$(1+z)^2 L_p = \frac{\delta_0^4 \beta_s^2 L}{9}. \quad (20)$$

In principle, Eq. (20) could be used to estimate the typical L of the ambient light of SHBs. However, the results for L_p are often reported for binning times much larger than the peak rise-times (e.g., Gehrels et al. 2006) and cannot be used to estimate L . For an SHB with N_{CB} prominent pulses of similar properties, the isotropic-equivalent energy, E_{iso} , is (DD2004):

$$E_{iso} = \frac{\delta_0^3 L \beta_s N_{CB}}{6c} \sqrt{\frac{\sigma_T N_B}{4\pi}} = (1.2 \times 10^{50} \text{ erg}) N_{CB} \beta_s \left(\frac{\delta_0}{10^3}\right)^3 \frac{L}{10^{40} \text{ erg s}^{-1}} \sqrt{\frac{N_b}{10^{48}}}. \quad (21)$$

The typical E_{iso} of SHBs is a few 10^{50} ergs, with a wide spread between $10^{48} - 10^{52}$ erg (see e.g. Kann et al. 2008). The typical values $\delta_0 = 1400$, $\beta_s = 1/3$, $N_{CB} = 3$ and $N_B = 10^{48}$ yield the estimate, $L \sim 10^{40} \text{ erg s}^{-1}$, which is quite normal for the putative progenitors of SHBs.

3.7. Correlations between prompt emission observables

The pronounced dependence of LGRBs observables on the Doppler factor, that ranges over a broad domain, led to simple correlations between them (DD2000, DDD2004, DD2007a). Similar correlations between prompt emission observables are expected in SHBs if they are dominated by a single class of progenitors. But the scarcity of data and lack of statistics on SHBs with secured redshift do not yet allow conclusive tests of such correlations.

The simplest CB model correlations for single pulses are $\Delta t \propto E_p^{-1}$, and $E_{iso} \propto (1+z)^2 L_p^{4/3}$. They are well satisfied for LGRBs (DD2004). For other pairs of observables, the predicted correlations are slightly more elaborate (DDD2007a). For instance, given that $(1+z) E_p \propto \delta_0 \gamma_0$ and $E_{iso} \propto \delta_0^3$ one expects, $(1+z) E_p \propto E_{iso}^{1/3}$. But that is precise only for the low E_p and E_{iso} (large θ) cases, at the XRF limit of the LGRB distribution. For $\theta \lesssim 1/\gamma_0$,

$(1+z)E_p \propto \gamma_0^2$ and $E_{iso} \propto \gamma_0^3$ implying that $(1+z)E_p \propto E_{iso}^{2/3}$. Since the observer's angle varies continuously, XRFs and GRBs lie, in the $[(1+z)E_p, E_{iso}]$ log-log plane, close to a line whose slope varies smoothly from 1/3 to 2/3 (DDD 2007a), as shown in Fig. 5. In Fig. 5 we also show the limited observational information on the $[(1+z)E_p, E_{iso}]$ correlation for SHBs: The results, like those for LGRBs, are fitted to a power-law varying from a 1/3 to a 2/3 slope (DDD2007a):

$$(1+z)E_p \approx E_p^0 ([E_{iso}^\gamma/E_0]^{1/3} + [E_{iso}^\gamma/E_0]^{2/3}), \quad (22)$$

with two parameters E_p^0, E_0 . They are almost equally well fit by just the higher power. This is not surprising, for selection effects may imply that, so far, only the most energetic SHBs have been observed. SHBs viewed far off axis, are wider and should look like GRBs of low luminosity without an associates SN.

The correlations between E_p and other prompt observables (peak luminosity, peak rise-time, lag-time, and variability), which are satisfied for LGRBs (DDD2007a), are also very straightforward tests of the hypothesis of ICS for SHB produced by a single class of progenitors, but the data on SHBs are not precise enough to reach a conclusion at the moment.

4. The synchrotron radiation afterglow

As a CB plough through the ISM, its radiation ionizes the gas in front of it. In its rest frame, the ionized ISM particles impinge on the CB with a Lorentz factor γ and generate in it a turbulent magnetic field in equipartition with their energy density, $B \approx \sqrt{4\pi n m_p c^2} \gamma$. The swept-in electrons are Fermi accelerated by the CB's turbulent magnetic field and emit synchrotron radiation. The SR, isotropic in the CB's rest frame, has a characteristic frequency, $\nu_b(t)$, the typical frequency radiated by the electrons that enter a CB at time t with a relative Lorentz factor $\gamma(t)$. In the observer's frame:

$$\nu_b(t) \simeq \frac{\nu_0}{1+z} \frac{[\gamma(t)]^3 \delta(t)}{10^{12}} \left[\frac{n}{10^{-3} \text{ cm}^3} \right]^{1/2} \text{ Hz}. \quad (23)$$

where $\nu_0 \sim 8.5 \times 10^{15} \text{ Hz} \simeq 35 \text{ eV}$. The spectral energy density of the SR from a single CB at a luminosity distance D_L is given by (DDD2003a):

$$F_\nu \simeq \frac{\eta \pi R^2 n m_e c^3 \gamma(t)^2 \delta(t)^4 A(\nu, t)}{4 \pi D_L^2 \nu_b(t)} \frac{p-2}{p-1} \left[\frac{\nu}{\nu_b(t)} \right]^{-1/2} \left[1 + \frac{\nu}{\nu_b(t)} \right]^{-(p-1)/2}, \quad (24)$$

where $p \sim 2.2$ is the typical spectral index² of the Fermi accelerated electrons, $\eta \approx 1$ is the fraction of the impinging ISM electron energy that is synchrotron re-radiated by the CB, and $A(\nu, t)$ is the attenuation of photons of observed frequency ν along the line of sight through the CB, the host galaxy (HG), the intergalactic medium (IGM) and the Milky Way (MW):

$$A(\nu, t) = e^{-(\tau_\nu(\text{CB})+\tau_\nu(\text{HG})+\tau_\nu(\text{IGM})+\tau_\nu(\text{MW}))}. \quad (25)$$

The opacity $\tau_\nu(\text{CB})$ at very early times, during the fast-expansion phase of the CB, may strongly depend on time and frequency. The opacity of the circumburst medium [$\tau_\nu(\text{HG})$ at early times] is affected by the GRB and could also be t - and ν -dependent. The opacities $\tau_\nu(\text{HG})$ and $\tau_\nu(\text{IGM})$ should be functions of t and ν , for the line of sight to the CBs varies during the AG observations, due to the hyperluminal motion of CBs. These and the dependence of the synchrotron AG on $\nu_b(t)$ may generate complex chromatic behaviour in the AGs (DDD2007b).

The Swift X-ray bands are above the characteristic frequency ν_b in Eq. (23) at all times. It then follows from Eq. (24) that the *unabsorbed* X-ray spectral energy density has the form:

$$F_\nu \propto R^2 n^{(p+2)/4} \gamma^{(3p-2)/2} \delta^{(p+6)/2} \nu^{-p/2} = R^2 n^{\Gamma/2} \gamma^{3\Gamma-4} \delta^{\Gamma+2} \nu^{-\Gamma+1}, \quad (26)$$

where we have used the customary notation $dN_\gamma/dE \approx E^{-\Gamma}$. The ISM density in globular clusters and in the surrounding medium, if they are far off galactic center, may be low enough such that the optical band is also above the bend frequency ν_b , and then the optical AG is also described by Eq. (26) and the AG is achromatic all the way between the optical to the X-ray band with a spectral index $\beta_{OX} \simeq 1.1$.

4.1. The early time SR afterglow

During its early-time emission, when both γ and δ stay put at their initial values γ_0 and δ_0 , Eq. (24) yields an early time light curve $F_\nu \propto e^{-\tau_w} R^2 n^{(1+\beta)/2} \nu^{-\beta}$. If the progenitor is embedded inside a globular cluster or a super star cluster which blows a constant wind into the ISM or IGM with a density profile $n \propto 1/r^2 \sim 1/t^2$, the early time SR light curve as given by Eq. (24) has the form,

$$F_\nu \propto \frac{e^{-a/t} t^{1-\beta} \nu^{-\beta}}{t^2 + t_{exp}^2}, \quad (27)$$

²The normalization in Eq. (23) is only correct for $p > 2$, for otherwise the norm diverges. The cutoffs for the ν distribution are time-dependent, dictated by the acceleration and SR times of electrons and their ‘Larmor’ limit. The discussion of these processes being complex (DD2003a, DD2006), we shall satisfy ourselves here with the statement that for $p \leq 2$ the AG’s normalization is not predicted.

until the CB reaches the constant ISM or IGM density.

4.2. Jet breaks, missing breaks and asymptotic decay

As it ploughs through the ionized ISM, the CB gathers and scatters its constituent ions, mainly protons. These encounters are ‘collisionless’ since, at about the time it becomes transparent to radiation, a CB also becomes ‘transparent’ to hadronic interactions (DD2004). The scattered and re-emitted protons exert an inward pressure on the CB, countering its expansion. In the approximation of isotropic re-emission in the CB’s rest frame and a constant ISM density $n \sim n_e \sim n_p$, one finds that within a minute or so of observer’s time t , typical SHB generating CBs of baryon number $N_b \sim 10^{48}$ reach an approximately constant ‘coasting’ radius $R \sim 10^{14}$ cm, before they finally stop and blow up, after a journey of years of observer’s time. During the coasting phase, and in a constant density ISM, $\gamma(t)$ obeys (DDD2002a, DDD2006):

$$(\gamma_0/\gamma)^4 + (2\theta^2 \gamma_0^2 (\gamma_0/\gamma)^2) = 1 + 2\theta^2 \gamma_0^2 + t/t_0, \quad (28)$$

with

$$t_0 = \frac{(1+z) N_B}{8 c n \pi R^2 \gamma_0^3}. \quad (29)$$

As can be seen from Eqs. (28,29), $\gamma(t, t_0, \theta, \gamma_0)$, and consequently also δ , change little as long as $t < t_b \equiv [1 + 2\gamma_0^2 \theta^2] t_0$, where,

$$t_b = (1300 \text{ s}) [1 + 2\gamma_0^2 \theta^2] (1+z) \left[\frac{\gamma_0}{10^3} \right]^{-3} \left[\frac{n}{10^{-3} \text{ cm}^{-3}} \right]^{-1} \left[\frac{R}{10^{14} \text{ cm}} \right]^{-2} \left[\frac{N_B}{10^{48}} \right], \quad (30)$$

and they approach a power-law decay, $\delta \propto \gamma \sim t^{-1/4}$ for $t > t_b$. The slow change in γ and δ for $t \lesssim t_b$ produces the ‘plateau’ phase of canonical afterglows. Their asymptotic power-law decay for $t \gg t_b$, when inserted in Eq. (26), yields the asymptotic power-law decay (DDD2007b),

$$F_\nu(t) \sim t^{-\beta-1/2} \nu^{-\beta} = t^{-\Gamma+1/2} \nu^{-\Gamma+1}, \quad (31)$$

where $\beta \equiv \Gamma - 1 = p/2 \sim 1.1$. Eq. (31) is valid as long as the ISM has an approximately constant density. The gradual transition (‘break’) of the AG from the plateau phase to a power-law decay at $t \gtrsim t_b$ takes place when the CB has swept in a mass comparable to its initial mass. This CB model bend/gradual break is different from the achromatic break predicted by the conical Fireball model when the ejecta decelerate to a point when the observer begins to see the entire opening angle of a conical ejecta (Rhoads 1997,1999).

Density variations complicate the simple shape of AGs and will not be discussed here, except for noting that for an ISM with an approximate $\sim 1/r^2$ density profile, such as in a

globular cluster, or in a galactic halo with an isothermal sphere density profile, which CBs may reach late in their motion, or in a windy environment created around superstar clusters by their blowing winds, the predicted X-ray and optical AG has a simple power-law form:

$$F_\nu(t) \sim t^{-\beta-1} \nu^{-\beta} = t^{-\Gamma} \nu^{-\Gamma+1}. \quad (32)$$

In ordinary LGRBs, t_b is usually larger than a few hundreds of seconds but, in intrinsically bright LGRBs, in particular in those which happen to take place in a dense ISM environment, the break in the X-ray AG may occur before the end of the prompt emission. Such breaks may be hidden under the much brighter ICS emission and only the power-law decaying tail of the AG is observed (DDD2008b). In SHBs, the low density environment of globular clusters, in particular those with a large offset from the galactic center, yield relatively large t_b values as can be seen from Table II. For SHBs in young superstar clusters with a strong wind, the AG has the simple power-law decay given by Eq. (32) with no jet break.

5. The extended soft emission component

Globular clusters (GCs) are concentrations of $\sim 10^4$ to 10^8 stars in and around galaxies. (e.g. the GC 037-B327 in M31 has a mass $M_{GC} = (3 \pm 0.5) \times 10^7 M_\odot$, Ma et al. 2006), They are the environment wherein a considerable fraction of low-mass X-ray binaries (compact stars accreting from a companion), milli-second pulsars (neutron stars having been spun-up by accretion) and neutron star binaries are found. Since these are some of the putative progenitors of SHBs, it is natural to test whether some features of these bursts, other than their distribution relative to the host-galaxy center (Troja et al. 2007, Kann et al. 2008), are also compatible with a GC location. GCs have typical core radii of $r_c \simeq 1$ pc. Sometime they have an intermediate mass black hole at their center. Relatively large GCs have a core-luminosity density of $O(10^5 L_\odot \text{pc}^{-3})$ and a total luminosity L_{GC} of order $10^6 L_\odot \sim 4 \times 10^{39} \text{erg s}^{-1}$.

The more recently discovered (Arp & Sandage 1985) superstar clusters (SSCs) are star concentrations similar to GCs in their sizes, but denser, more massive, and more active. A good fraction of SSCs may be gravitationally bound and constitute a proto-globular cluster, thus the alternative denomination young globular clusters. Many active hosts harbour SSCs, including interacting galaxies, starburst galaxies and star-formation regions in normal spirals. Dust often obscures SSCs, which are not easy to see at optical frequencies, and have only recently been studied in detail with the HST, mostly in the Antennae galaxies (Whitmore et al. 1995), in M82 and in NGC 2553. The sizes of observed SSCs range from 1 to 6 pc, their masses from a few 10^4 to $10^6 M_\odot$ and their luminosities from 10^{40} to $10^{42.5} \text{erg s}^{-1}$,

nearly $10^9 L_\odot$ (Melo et al. 2005 and references therein). Even at small redshifts, active SSCs are not a rare phenomenon; they must have been rather common in the past. Because of their enhanced stellar-evolution activity, SSCs are even more natural hosts than GCs for the putative progenitors of SHBs.

We shall argue that the extended soft component observed in a good fraction of SHBs is due to ICS of the light of a superstar cluster by the CBs crossing it, after they have left the close-by luminous environment generating the SHBs prompt peaks, or SR in young superstar clusters with a very large ($n \sim 10^3 - 10^6 \text{ cm}^{-3}$) ISM density. This is supported by the typical duration and isotropic energy of ESECs which are compatible with the said hypothesis. Concerning the ESECs spectrum, the data are only sufficient to conclude that the hypothesis is consistent.

5.1. The duration of an ESEC

For the measured average SHB redshift, $z \sim 0.5$, and with the typical values, $\delta_0 \gamma_0 \sim 1400$, the distance travelled by a CB in the typical $t_{ESEC} \sim 100$ s duration of an ESEC is $x \sim \gamma_0 \delta_0 c t_{ESEC} / (1+z) \approx 1.2$ pc, coincident with the typical core radius of a GC or SSC. This straightforward understanding of ESEC durations is independent of whether the mechanism generating the radiation is ICS or SR, provided the sources are CBs, moving relativistically, and not significantly decelerating in this short interval of observers time.

5.2. The ICS contribution to the ESEC

As a CB moves through the light of the a host star cluster its ICS produces a light curve which traces the density of the light along the CB trajectory. This light is a sum of a smooth background light from all the stars in the cluster plus light peaks from the passage near very luminous stars. For simplicity, consider the contribution to the ESEC light curve from ICS of background light by a CB ejected near the center of an SSC. It is obtained simply by replacing the typical energy ϵ_g and density $n_g(t)$ of the glory photons in the expression describing the prompt SHB with, respectively, the typical energy ϵ_c and the density $n_c(t)$ of the GC background photons, where $n_c(0) = 3 L_{ssc} / 4 \pi c \epsilon_c r_c^2$ and L_{ssc} is the SSC luminosity. The resulting ESEC light curve is given by Eqs. (11) and (6) with Δt replaced by $\Delta t_c = r_c (1+z) / c \gamma_0 \delta_0$. The isotropic-equivalent energy of the ESEC is then given by,

$$E_{iso}[ESEC] \approx \sigma_T N_b N_{CB} \gamma_0 \delta_0^3 \frac{3 L_{ssc}}{4 c r_c} \sim (10^{49} \text{ erg}) \frac{N_b}{10^{48}} \frac{N_{CB}}{4} \frac{pc}{r_c} \frac{\gamma_0 \delta_0^3}{1400^4} \frac{L_{ssc}}{10^8 L_\odot}. \quad (33)$$

The result of Eq. (33) is of the observed order of magnitude, but has more sources of accumulated uncertainty and variability than other CB-model results.

The ESEC after transparency time, for a spherical SSC, is a decreasing function of time from the beginning, if the progenitor is in the front hemisphere, and the CBs' distance from the GC increases. Otherwise, the ESEC light curve first increases and then decreases with time. The data are consistent with these expectations, but so far insufficient to test them in detail.

5.3. The SR contribution to the ESEC

Some young superstar clusters have a very large ISM density, $10^3 \lesssim n \lesssim 10^6 \text{ cm}^{-3}$. Consequently, the emission rate of SR radiation from CBs moving inside such SSCs, which is proportional to the ISM density (see Eq. (24)), is very intense and relatively hard with a spectral index $\beta \simeq 1/2$, because $\nu_b \propto n^{1/2}$ (see Eq. (23)) is well above the X-ray band. At early time it is given by Eq. (27) with $\beta \simeq 1/2$. As soon as the CB escapes out of a dense core of a superstar cluster, the density decreases fast like $1/r^2$, and the light curve decreases rapidly and becomes softer with its spectral index increasing to $\beta \approx 1.1$,

$$F_\nu \propto \frac{e^{-a/t} t^{1/2} \nu^{-1/2}}{t^2 + t_{exp}^2} \rightarrow t^{-2.1} \nu^{-1.1}. \quad (34)$$

Eq.(34) is valid when the CBs encounter a very large density inside the SSC such that the CBs reach their coasting radius, $R_{cb} \propto N_b^{1/3} n^{-1/3} \gamma_0^{-2/3}$, well inside the SSC and $t_{exp} \ll \Delta_{ssc}$.

6. Comparison between SHB afterglows and their CB model description

6.1. General

To date, Swift has detected over 30 SHBs, localized them through their γ , X-ray and UVO emissions and followed them until they faded into the background, usually within less than a day or two. A few deep observations of the X-ray emission of several SHBs at later times were made with Chandra. Several additional SHBs were localized by the Inter Planetary Network (IPN) to much larger error boxes and a couple more by HETE. Beside the Swift UVO observations, there have been many optical follow-up measurements of SHBs by ground-based optical telescopes including some of the largest ones. In order to demonstrate the success of the CB model to explain SHBs, we have limited the detailed comparison between theory and observations to all SHBs (15) whose X-ray and/or optical AG were well

sampled. The *a-priori* unknown parameters are the number of CBs, their ejection time, baryon number, Lorentz factor and viewing angle, and the distributions of the glory’s light and the ISM density along the CBs’ trajectory.

In more than 2/3 of the SHBs detected by Swift, no ESEC was detected and only in few SHBs were its light curve and spectrum measured. Several SHBs have no measured redshift. So far no absorption or emission lines were detected in the afterglow of SHBs due to their faintness (Stratta et al. 2007). Their redshifts listed in Table I were determined from their host galaxies or from the nearest bright galaxy or galaxy cluster if no galaxy or only extremely faint galaxies were found in their XRT error circles. But, the lack of secured redshifts and well measured ESECs does not prevent other critical tests of the CB model predictions, which are insensitive to the unknown redshift and the detailed behaviour of the ESEC.

We have assumed quite generally an isothermal sphere density profile, $n \propto 1/(r^2+r_c^2)$, for both the star clusters and galactic halos, with $r_c \sim O(1 pc)$ for GCs and SCCs, and $r_c \sim O(10 kpc)$ for galactic halos, until being taken over by a constant-density ISM or IGM, respectively. This density profile describes also the windy density profile outside young superstar clusters or SN remnants, created by the strong winds from SSCs or the progenitor star of core collapse SNe, respectively.

Because of the short duration of SHBs and the fast initial expansion of the CBs, we have assumed that by the time they have escaped from the globular/superstar cluster, they have merged into a single CB. This reduces dramatically the number of fitted parameters without affecting the quality of the fits. Flares during the fast decay phase of the extended soft emission component (ESEC) or the afterglow phase due to late CB ejections are superimposed on the smooth light curve. To demonstrate that the CB model correctly describes all of the observed features of the Swift X-ray observations, it suffices to include in the fits only the latest observed pulses or flares during the ESEC. This is because the last exponential factor in Eq. (18) suppresses very fast the relative contribution of earlier pulses by the time the data sample the later pulses or flares.

The X-ray light curves reported in the Swift/XRT GRB lightcurve repository (Evans et al. 2007) were fitted with use of Eq. (11) for ICS pulses and Eq. (24) for their synchrotron contribution, with an early time behaviour as given by Eq. (27).

Below we summarize the observations and CB model description of all the SHBs with well sampled X-ray light curve, reported in the Swift/XRT GRB lightcurve repository (Evans et al. 2007). and/or optical light curve. The CB model predictions are based on Eq. (11) for the prompt emission and the fast decay phase, Eq. (14) for the evolution of the spectral index

during the decay of the prompt emission or Eq. (15) for the hardness ratio, and Eq. (24) for the SR afterglow. The hardness ratio during the SR dominated phase was fitted by a constant. The best fit parameters used in their CB model description are reported in Table II. Also reported there are the CB model fit parameters of the flares (subscript f) superimposed on the smooth XRT and/or optical light curves. Due to their faintness, in most cases the AGs of SHBs are not well measured beyond the plateau phase. This does not allow a reliable estimate of p or the density profile from the late temporal decay of the AG. In such cases we have fixed p to have its canonical theoretical value, $p=2.2$, and indicated that by (2.2) in Table II.

6.2. Case Studies

SHB 050709.

a. Observations: This SHB, which was localized by HETE (Vilasenor et al. 2005), was relatively very faint ($E_{iso} \sim 2.4 \times 10^{48}$ erg). It had a multi-spike peak with $T_{90} = 70 \pm 10$ ms in the 30-400 keV band, $T_{90} = 220 \pm 50$ ms in the 2-25 keV band, and showed a fast hard to soft spectral evolution with $E_p \sim 86 \pm 16$ keV and a photon spectral index $\Gamma = 0.82 \pm 0.13$. A soft extended emission component was detected 24 s after burst with $T_{90} = 130 \pm 7$ s, $\Gamma = 1.98 \pm 0.18$, and a fluence much larger than that of the short burst, unlike what is seen in the giant flares of SGRs. It was the first SHB for which an optical AG was discovered and was used to localize it in a star forming dwarf galaxy at redshift $z = 0.16$ (Hjorth et al. 2005a, Fox et al. 2005, Covino et al 2006) at a projected distance of ~ 3.8 kpc from its center. Its X-ray AG was detected by Chandra (Fox et al. 2005). Its optical light curve as measured by Watson et al. (2006) is shown in Fig. 1a.

b. Interpretation: The short burst shows all the properties expected from ICS of glory light by a jet of CBs with a relatively small baryon number emitted by the source. The spectral index of the extended soft emission component (ESEC), $\Gamma = 1.98 \pm 0.18$, the lack of spectral evolution during the ESEC and the duration of the ESEC are consistent with those expected from SR ($\Gamma \sim 2.1$) of CB propagating in a $r_c \sim 1 pc$ core of a globular cluster and $t \sim (1+z)r_c/c\gamma_0, \delta_0 \sim 120$ s). The optical afterglow is well explained by a CB propagating out of the dwarf galaxy with an isothermal sphere density distribution $n \propto 1/(r^2 + r_0^2)$, as demonstrated in Fig. 1a.

SHB 050724.

a. Observations: This burst at redshift $z = 0.257$ was studied in detail in Campana et al. 2006b, Grupe et al. 2006 and Malesani et al. 2007. The BAT on board Swift triggered on the burst at 12:34:09 UT on 2005, July 24. The burst had $T_{90} = 3.0 \pm 1.0$ s, but most of

the energy of the initial SHB was released in a hard spike with a duration of 0.25 s. The bulk of the burst energy was not emitted in the short initial spike but in an extended soft emission component with $\Gamma = 2.5 \pm 0.2$ which lasted ~ 150 s. Swift’s XRT began observing the afterglow 74 s after the BAT trigger. The Chandra X-ray observatory performed two observations, two days and about three weeks after the burst. The complete X-ray light curve is shown in Fig. 1b. It has the canonical shape observed in long GRBs, namely, a rapid decay with a fast spectral softening ending with a sharp transition to a plateau phase with a much harder power-law spectrum, $\Gamma = 1.79 \pm 0.12$ as shown in Fig. 1c. The AG steepens gradually into a late power-law decay. A large flare superimposed on the canonical light curve occurred around 50 ks after burst with a fluence of $\sim 7\%$ of that of the prompt burst. The flare has been detected also in the optical and NIR bands (e.g., Malesani et al. 2007). Spectral analysis of the XRT data (Campana et al. 2006b) showed no evolution during the afterglow phase, including the large late flare. Spectral analysis of the Chandra observations from the fading tail of this flare confirmed this result (Grupe et al. 2006). The burst took place 2.5 kpc (in projection) from the center of an elliptical host galaxy (Malesani et al. 2007).

b. Interpretation: The CB model X-ray light curve of SHB 050724 and its spectral index ‘light curve’ are shown in Figs. 1b,c. The early time emission is described by ICS of the progenitor’s glory light, the ESEC by ICS of the light of the core of the assumed superstar cluster or a globular cluster environment. The fast decay of the X-ray light curve and the rapid spectral softening took place when the CB was moving away from the quasi-isotropic light distribution in the dense stellar environment of the progenitor into the ISM of its elliptical host galaxy. As can be seen in Figs. 1b,c, this fast decay and spectral softening stopped simultaneously when the AG was taken over by the SR from the decelerating CB in an ISM of a constant density. As expected, apart from normalization, the late-time SR afterglow is similar in shape to the SR afterglow of LGRBs. Also the late flare superimposed on the canonical light curve is similar to those observed in many LGRBs. It was produced by enhancement of the emitted SR when the CB encountered a density bump in its voyage through the host’s ISM. The Chandra data show that the canonical AG continued to decay after the flare with the same slope and the same spectral index, $\beta_X = 0.79 \pm 0.15$. As shown, in Fig. 1b, the complete XRT light curve is well fit by the CB model. Moreover, the CB model relation $\alpha = \beta_X + 1/2 = p/2$ is well satisfied. The temporal behaviour of the canonical AG was best fit with $p = 1.56$, implying an unabsorbed spectral index, $\beta_X = p/2 = 0.78$, and an asymptotic power-law decay with a power-law index, $\alpha = \beta_X + 1/2 = 1.28$, in agreement with those observed.

The elliptical host galaxy of SHB 050724 was argued to provide strong support for a neutron star merger origin of this SHB. But, it was pointed out that neutron star mergers do

not produce the late accretion episodes needed in the standard folklore to power a late central activity which could produce the large flare around 50 ks after burst (Grupe et al. 2006). In the CB model, a late flare with a typical SR spectrum and little spectral evolution is produced by density bumps along the CB trajectory in the ISM. Such flares neither rule out nor support any specific origin of the SHB.

SHB 051210.

a. Observations: This was a faint two-spiked SHB localized by Swift. It had $T_{90} = 1.27 \pm 0.05$ s and no soft extended emission was detected (La Parola et al. 2006). The BAT spectrum was fit with a power-law with a photon spectral index $\Gamma = 1.1 \pm 0.3$. The XRT started observation 79 s after the BAT trigger. It detected a rapidly decreasing light curve, shown in Fig 1d, with a small flare superposed around 134 s. A possible host galaxy was discovered within the XRT error circle (Bloom et al. 2005a), but no emission or absorption lines were detected. No optical afterglow was detected.

b. Interpretation: The spectrum of the burst is consistent with ICS of glory light ($\Gamma \sim 1$ for $E \ll E_p$). The fast declining XRT light curve was fit as the tail of an ICS flare. The data are insufficient for a critical test of the CB model interpretation.

SHB 051221A.

a. Observations: This burst was discussed in detail in Soderberg et al. 2006a and Burrows et al. 2006. It was an intense, multi-spiked burst localized by Swift, The burst was also detected by Konus-Wind, Suzaku, INTEGRAL and RHESSI and its late afterglow by Chandra. The burst had $T_{90} = 1.4 \pm 0.2$ s, $\Gamma = 0.92 \pm 0.13$, and showed no signs of extended emission. The Swift/XRT observations of its X-ray light curve began 88 s after the Swift/BAT trigger. Its late time X-ray emission was also detected by Chandra. The measured X-ray light curve (Fig. 1e) of SHB 051221A shows the canonical behaviour of X-ray light curves of LGRBs (Nousek et al. 2005) with an asymptotic decay index $\Gamma \approx 2$. Its afterglow was detected also in the NIR, and optical bands. and was localized near the center (~ 1 kpc in projection) in a star forming galaxy with $z = 0.546$.

b. Interpretation: The prompt SHB was produced by ICS of glory light as evident from its spectral index $\Gamma \sim 1$. The XRT light curve is well fit by the SR tail of prompt flares taken over by the canonical SR afterglow emitted by a CB moving in a constant density ISM of the host galaxy, as shown in Fig. 1e. Its late afterglow with $\alpha = 1.6 \pm 0.05$ and $\Gamma = 1.97 \pm 0.13$ are consistent within errors with the CB model prediction, $\alpha = \Gamma - 1/2$. The wiggling of the light curve around the smooth theoretical line can be due to density variations along its trajectory, as was observed in afterglows of many LGRBs.

SHB 051227.

a. Observations: This was a multi-peaked burst with a bright X-ray afterglow localized by Swift (Barbier et al. 2005). It was initially thought to be LGRB, since it has $T_{90} = 8.0 \pm 0.2$ s (Hullinger et al. 2005), but a spectral analysis that showed a negligible spectral lag and a broad softer bump between 30 and 50 s were claimed to indicate an SHB (e.g. Kann et al. 2008). An exceedingly faint optical afterglow was discovered within the XRT error circle (Malesani et al. 2005a,b) with the VLT and also detected by Gemini.

b. Interpretation: The prompt burst is consistent with ICS of glory light ($\Gamma \sim 0.91 \pm 0.28$). The XRT light curve is consistent with an SR tail of a prompt emission taken over by a canonical SR afterglow, as shown in Fig. 1f. The XRT does not shed light on whether this GRB was or was not an SHB. Due to a gap in the data between 400 s and 4000 s, the theoretical shape and the values of the SR afterglow parameters are uncertain.

SHB(?) 060121.

a. Observations: This intermediate duration GRB was discussed in detail in Donaghy et al. 2006, de Ugarte Postigo et al. 2006 and Levan et al. 2006. It was localized by HETE-2. It consisted of two peaks with $T_{90} = 1.60 \pm 0.07$ s at high energies, which were followed by a faint soft emission for several hundreds of seconds. It was also detected by Konus-Wind, Suzaku and RHESSI. Follow-up observations by Swift began 3 h after the burst. Its XRT-light curve is shown in Fig. 1f. Its faint optical afterglow was discovered by Malesani et al. (2006), which led to the discovery of its extremely faint host galaxy (Levan et al. 2006). The burst outshined its host galaxy (by a factor > 100). A photometric redshift for this event placed it at a most probable redshift of $z = 4.6$, with a less probable $z = 1.7$. In either case, GRB 060121 could be the farthestmost short GRB detected to date with an isotropic-equivalent energy release in gamma rays comparable to that of LGRBs.

b. Interpretation: Its intermediate duration and its unusual large redshift $Z = 4.7$, relatively small $E_p \approx 120$ keV, large equivalent isotropic gamma ray energy, $E_{iso} \approx 2.2 \times 10^{53}$ erg (or $E_{iso} \approx 4.3 \times 10^{52}$ erg for $z = 1.7$), vicinity (~ 2 kpc) to the center of the host galaxy, and its bright optical afterglow, suggest that GRB 060121 may have been an ordinary LGRB, and was wrongly classified as SHB. In Fig. 2a we show the CB model fit to its late AG, which, although satisfactory, does not shed light on its true identity.

SHB 060313.

a. Observations: This unusual burst was reported and discussed in detail in Roming et al. 2006. It was detected by Swift, Konus-Wind and INTEGRAL. It was a very intense burst, with many short spikes each with FWHM smaller than 20 ms, with $T_{90} = 0.7 \pm 0.1$ s. It had a very unusual average initial photon index, $\Gamma = -0.33(-0.29, +0.25)$ below the spectral peak during the initial 0.192 s of the burst (Golenetskii et al. 2006a). It had the highest fluence and the highest observed peak energy of all SHBs observed by Swift. No extended soft

emission was detected. Swift XRT detected its X-ray afterglow 79 s after the BAT trigger and measured its light curve until 200 ks (Fig. 2b) with a late afterglow photon index of $\Gamma = 1.96 \pm 0.09$. The XRT light curve shows flaring activity superimposed on a canonical light curve during the first 1000 s after burst. The optical afterglow of SHB 060121 was detected and followed by the Swift UVOT and by the VLT following its localization by Swift UVOT. A very faint host galaxy was detected at the afterglow position by Berger et al. (2006a).

b. Interpretation: The unusual early light curve and spectrum of SHB 060313, suggest an unusual progenitor and environment of this unusual SHB. In the framework of the CB model, the large number of short pulses requires a progenitor which fires many small CBs like a shot gun (Plaga, private communication) or a machine gun, rather than a cannon. The unusual hard spectrum could be produced by inverse Compton scattering of self absorbed radiation produced inside the CBs. In contrast to the unusual prompt emission, the afterglow is not unusual, and can be well explained as SR radiation from a CB propagating in a constant density ISM of the host galaxy, as shown in Fig. F2b.

SHB 060801.

a. Observations: This SHB was detected and localized by Swift (Racusin et al. 2006a) and was also detected by Suzaku. It had $T_{90} = 0.5 \pm 0.1$ s. It consisted of two pulses which peaked 60 ms and ~ 100 ms after their beginning (Sato et al. 2006). No extended soft emission was detected. The XRT began taking data 63 s after the BAT trigger (Racusin et al. 2006b). The 0.3-10 keV X-ray light curve shows a plateau from 73 s until 115 s after the BAT trigger, which turns into an exponential decay. The X-ray emission was not detected after 1000 s. Follow up optical observations did not detect an optical afterglow. A single galaxy lying within the XRT error box at redshift $z = 1.1304$ was suggested as its host galaxy, making SHB 060801 the most distant SHB with a secured redshift.

b. Interpretation: The prompt emission pulses are well explained by ICS of a thin bremsstrahlung glory of two CBs. The extended soft emission at redshift 1.13 was too dim to be detected by BAT, but its ending and decay probably are the emission detected and followed with the XRT. In the CB model it is well described by ICS of the GC's light when the CBs leave its dense core and move into the surrounding ISM, as shown in Fig. 2c.

SHB 061006.

a. Observations: The Swift observations of this burst are reported in Schady et al. 2006. This burst began with an intense double spike which lasted 0.5 s. The SHB was also detected by RHESSI, KONUS-WIND and Suzaku (Hurley, et al. 2006). It was followed by an extended soft emission with $T_{90} = 130 \pm 10$ s. The XRT began follow-up observations at 143 s after burst. The XRT light curve (Fig. 2d) initially decayed with a slope of $\alpha = 2.3 \pm 0.3$, followed by a shallow slope beginning at 300 s with a spectral index $\Gamma = 1.7 \pm 0.3$. VLT observations

(Malesani et al. 2006b) found a faint source that was subsequently found to fade, revealing a starforming host galaxy (Malesani et al. 2006c, Berger et al. 2006b) at redshift $z=0.4377$. The burst location is about 8 kpc from the galactic center.

b. Interpretation: In the CB model, the prompt pulses can be explained by ICS of glory light of the SHB progenitor. The extended soft emission could be produced by synchrotron radiation from the CBs while they were crossing the superstar cluster where the SHB took place. As shown in Fig. 2d, the initial decay of the XRT light curve can be explained by SR emission from the CBs while it was crossing the SSC wind, whereas the shallow decaying AG is the afterglow emitted when the CBs propagate in the ISM surrounding the SSC.

SHB 070714B.

a. Observations: The Swift observations of this SHB are detailed in Racusin et al. 2007. The SHB was a very bright multi-spiked event lasting about three seconds which was followed by soft extended emission that lasted 64 ± 5 s. Swift/XRT began follow-up observations 61 sec after trigger. A joint Swift - Suzaku spectral analysis yielded a hard spectrum and a high peak energy (Ohno et al. 2007). The photon spectral index integrated over the SHB was $\Gamma = 0.99\pm 0.08$. The 0.3-10 keV light curve (Fig. 2) showed the canonical behaviour observed in LGRBs, namely, a steep decay with super-imposed flares taken over around 400 s by an afterglow that gradually bends over into an asymptotic power-law decay with $\alpha\sim 1.6$. The fast decay of the soft extended emission was accompanied by a rapid spectral softening (Fig. 2f) until the plateau phase took over. The photon spectral index during the AG phase was $\Gamma = 1.95\pm 0.15$ (Zhang et al. 2007). An optical afterglow was discovered 10 minutes after the GRB by the Liverpool Telescope (Melandri et al. 2007), which led to the discovery of a host galaxy at a redshift $z=0.92$ (Graham et al. 2008).

b. Interpretation: The initial fast decay and rapid spectral evolution of the early time X-ray light curve of SHB 070714B, are well reproduced by the CB model (Figs. 2e,f. The data beyond 400 s show a considerable flaring activity. This makes quite uncertain the CB model best fitted parameters of the smooth SR afterglow component, reported in Table II.

SHB 070724A.

a. Observations: This short burst was a faint single-spiked GRB with $T_{90} = 0.40\pm 0.04$ s localized by Swift with no detected ESEC (Ziaeeepour et al. 2007). Swift XRT began its observations of the burst X-ray afterglow 72.1 s after trigger and followed its rapid decay and two superimposed X-ray flares peaking around 127 s and 200 s. The fast decay of the AG turned into a shallow decay around 400s which steepened around 40 ks. A faint source at redshift $z=0.457$ within the XRT error circle was suggested as a possible star forming host galaxy. Deep imaging and image subtraction did not reveal an optical afterglow. An analysis of the BAT data yielded $E_p\sim 41$ keV and a photon index of $\Gamma = 2.2$.

b. Interpretation: The CB model fit to the XRT light curve is shown in Fig. 3a. The light curve is well fitted by two ICS pulses taken over by an SR afterglow from a CB moving in a constant low-density ISM. The relatively large value, $\gamma\theta$ indicates nearly a ‘far off axis’ SHB consistent with its relatively small E_{iso} and E_p and a large pulse width compared to those of ordinary SHBs.

SHB 071227A.

a. Observations: This short burst was detected and localized by Swift (Sakamoto et al. 2007, Sato et al. 2007). It was also observed by Suzaku and Konus-Wind. The SHB was a multi-peaked structure with a duration of about 1.5 seconds and a time averaged power-law spectrum with a photon spectral index $\Gamma = 1.2 \pm 0.2$. The Swift XRT began observing GRB 071227 79.5 seconds after the BAT trigger. The XRT light curve shows the canonical behaviour: soft flares superposed on a decaying light curve which changes to a fast decay with a spectral softening, until it is taken over by a plateau/shallow decay around 1000 seconds.

b. Interpretation The CB model fit to the XRT light curve is shown in Fig. 3c. The light curve and spectral evolution are well fitted by ICS of a GC light of a CB moving away from the GC into a constant low-density ISM where the AG is dominated by SR emission. However, the data after the fast decay phase are scarce and constrain only weakly the CB model parameters of the SR afterglow.

SHB 080123.

a. Observations: This short burst was detected and localized by Swift. The Swift observations of this burst are reported in detail in Ukwatta et al. 2008 and Copete et al. 2008. Its light curve shows two well-separated peaks. The first started at 0.3 s and is no wider than 64 msec. The second peak started at 0.6 s with a FRED-like shape and a duration of 256 ms. Its soft extended emission lasted 120 s after the prompt hard emission of the short GRB and included soft flares (Copete et al. 2008). The XRT observations started 108 s after the BAT trigger. The XRT light curve (Fig. 3d) shows the canonical behaviour: a fast decay with a rapid spectral softening, which was taken over by a plateau/shallow decay around 500 s with a typical photon index of $\Gamma = 2.1 \pm 0.2$.

b. Interpretation: The fast decay of the XRT early time light curve and its rapid spectral softening (not shown here) are well fit by ICS of light from a GC/SSC. It is being taken over around 500 s by a plateau/shallow decay with a typical photon index of $\Gamma = 2.1 \pm 0.2$ which is well fit by SR emission from a CB deceleration in a a medium of low constant density (Fig. 3d). The scarce data on the late afterglow constrain only weakly the CB model parameters of the SR afterglow.

SHB 080503.

a. Observations: This short burst was detected and localized by Swift. The Swift observations of this burst are reported in detail in Mao et al. 2008. Its light curve (Fig. 3e) shows an initial spike starting at 0.1 s after the BAT trigger with a fast rise to a peak at 0.2 s, then, a roughly exponential decay down to background at 0.7 s. It had an extended soft emission which started at about 10 s, rose with two peaks at 26 s and 37 s, and then fell to background levels at 220 s. The Swift XRT began observing SHB 080503 81 s after the BAT trigger. The XRT light curve showed an exponential decay with a gradual spectral softening from $\Gamma \sim 1$ at the beginning of the XRT observations to $\Gamma \sim 3$ around 500 s. The X-ray AG (Fig 3e) decreased below the Swift detection sensitivity around 1000 s after burst, but was detected later between 4.29-4.66 days after burst by Chandra (Butler et al. 2008). A rising optical afterglow was detected on the second night after trigger by Perley et al. (2008a) with Gemini-North. Continuous monitoring of this optical counterpart on consecutive nights (Bloom et al. 2008, Perley et al. 2008b) found no further re-brightening and its fading (Fig. 3f). The OT was not detected with HST 9.2 days after the BAT trigger (Perley et al. 2008c).

b. Interpretation: The exponential decay of the XRT light curve at the end of the ESEC is well described by ICS of a CB emerging from the dense stellar core of a superstar cluster of a typical core radius $r_c \sim 1$ pc, as shown in Fig. 3e. This is supported by the rapid spectral softening/decreasing hardness ratio during this decay. The decay is stretched over $t > 900$ s, probably because of a relatively large redshift and a very low surrounding density which results in a very faint X-ray synchrotron afterglow and a delayed take-over time. The low extra cluster density yields a prolonged expansion time of the CB, $t_{exp} \approx 7553$, in Eq. (34) and an initially rising SR afterglow (Fig. 3f). The asymptotic decay of the optical AG is well described by $F_\nu \propto t^{-(1+\beta)}$ (Fig. 3f) with $\beta = \beta_X \approx 1.1$, typical of a SR emitted by a CB moving in the wind of a young superstar cluster (a proto globular cluster). A superstar cluster environment of the SHB is supported by the general properties of its ESEC.

GRB 060614.

a. Observations: This puzzling GRB was discussed in detail in Gehrels et al. 2006, Gal-Yam et al. 2006 Cobb et al. 2006, and Mangano et al. 2008. Swift-BAT triggered on GRB 060614 on 2006 June 14 at 12:43:48 UT. The BAT light curve showed a 5 s series of short hard peaks followed by a fainter, softer and highly variable extended prompt emission with $T_{90} \sim 102$ s. Konus-Wind was also triggered by GRB 060614, about 4 s after the BAT trigger. For the initial group of short hard peaks it measured $E_p \sim 300$ keV. The XRT and UVO aboard Swift started observation 97 s after the BAT trigger which continued up to 51 days after burst The X-ray light curve showed the canonical behaviour observed in many LGRBs and in practically all SHBs, i.e. initial fast decay with a rapid spectral softening

which is taken over by a plateau that later bends into an asymptotic power-law decay. The AG bend/break started around 30 ks and the asymptotic temporal decay had a power-law index $\alpha = 2.1 \pm 0.07$. The burst was located at the outskirts of a faint starforming galaxy at redshift $z = 0.125$. Very deep searches (Gal-Yam et al. 2006 Mangano et al. 2008) did not discover an associated SN.

b. Interpretation: The initial short peaks of GRB 060614, the lack of an associate SN akin to those discovered in ordinary LGRBs, the strict limits on lag-times in its early short pulses, its extended soft emission (well fit by a power-law spectrum with a photon index $\Gamma = 2.13 \pm 0.05$) and its low isotropic energy $((2.5 \pm 0.7) \times 10^{51}$ erg; Mangano et al. 2008) are typical of SHBs. On the other hand, the long $T_{90} \sim 5$ s of its initial complex of short pulses, its $(1+z)E_p \sim 440$ (–281, +923) keV, and its location inside a starforming galaxy are typical of LGRBs. Various solutions of these apparent contradicting pieces of evidence were suggested. Gal-Yam et al. 2006 and Gehrels et al. 2006 suggested that GRB 060614 (and GRB 060505) belongs to a new class of long GRBs. Cobb et al. (2006) suggested that its location in a the nearby host galaxy could be a chance coincidence. Dado et al. (2008) suggested that GRB 060614 could be produced by an extremely faint core collapse supernova or by a “failed supernova” - the original collapsar model (Woosley 1993).

Our CB-model analysis indicates that GRB 060614 probably was a very hard and energetic SHB in a very bright SSC which was viewed far off axis ($\gamma\theta \sim 3.08$). Its relatively large viewing angle yielded a relatively small Doppler factor δ which stretched the observed durations of its prompt emission pulses and its extended soft emission component relative to those of ordinary SHBs, and decreased their peak emission energy, equivalent isotropic energy and peak luminosity.

In Fig. 4a we present the CB model fit to the canonical X-ray light curve of GRB 060614. The decay of the ESEC is very well described by ICS of the light of a superstar cluster as the CB leaves the cluster and enters the ISM. Figs. 4b,c,d compare the observed hardness ratio, evolution of the effective photon spectral index and the evolution of E_p during the fast decay phase of the ESEC and the CB model predictions. The agreement between theory and observations is quite satisfactory. The XRT data on the decay of the prompt ICS emission extended only up to 480 s. The CB model estimates that it was taken over by SR only around 950 s. The second orbit XRT data began only at 4.5 ks after the BAT trigger but clearly show a stretched plateau until 30 ks when it begins to bend into an asymptotic power-law temporal decay. The plateau phase and the late decay of the X-ray afterglow are those expected for an SR afterglow from CB decelerating in an isothermal sphere density profile, $n \propto 1/(r^2 + r_s^2)$, namely $F_\nu \sim t^{-(1+\beta_X)} \nu^{-\beta_X}$ with $\beta_X \approx 1.1$ Such a density profile is encountered by CBs which move from inside the host galaxy into its halo. The CB model

best fit value, $\gamma_0 \theta = 3.08$, is typical of XRFs, which, in the CB model, are interpreted as far off-axis GRBs (e.g., DD2004, DDD2004). The corresponding value, $\delta = 2\gamma/(1+\gamma^2\theta^2) \approx \gamma/5$, yields E_{iso} and L_p which are, respectively, ~ 125 , and 625 times smaller than when they are measured at a typical viewing angle, $\theta \approx 1/\gamma_0$.

7. Summary and main conclusions

We have demonstrated that the entire observational data on SHBs can be explained by the assumption that SHBs are produced by highly relativistic jets ejected in processes involving compact stars, such as mergers of compact stellar objects, large-mass accretion episodes onto compact stars in close binaries or onto intermediate-mass black holes in dense stellar regions, and phase transition of compact stars. Natural environments of such events are the dense cores of globular clusters or superstar clusters and young supernova remnants. We have demonstrated that the cannonball model of GRBs can reproduce the main observed properties of their prompt emission, extended soft emission component and afterglows. In particular, we have used the CB model to fit the XRT light curve of all Swift SHBs with a well sampled X-ray afterglow. We have shown that their prompt gamma-ray emission is well described by inverse Compton scattering of the progenitor’s glory light, their extended soft emission component by ICS of light of the host star cluster or by synchrotron radiation in the high density interstellar medium of superstar cluster, and their afterglow by synchrotron radiation outside the cluster. We have also demonstrated that nearby GRBs of low luminosity short end of the duration distribution of LGRBs and without an associated SN, such as GRBs 060614 and 060505, may be SHBs viewed far off axis. The BATSE observations on board CGRO indicated that nearly *sim*25% of all GRBs are SHBs. The evidence from INTEGRAL that the rate of LGRBs is comparable to that of SNe of type Ib/c, which are a significant fraction of all core collapse SNe, implies that also the production rate of SHBs is large and comparable to the birth-rate of neutron stars. Hence neutron star merger, which has a rate much smaller than the birth-rate of neutron stars, cannot be the main source of SHBs. A high rate of SHBs (most of which are beamed away from us), comparable to that of SNe Ib/c, suggests that phase transition in neutron stars or mass accretion episodes onto stellar and intermediate mass black holes are more probable sources of SHBs.

Acknowledgment: We would like to thank A. De Rújula for a long and fruitful collaboration and for his contributions to this manuscript. A.D. would like to thank the Theory Division of CERN for its hospitality during this work.

REFERENCES

- Arp, H. & Sandage, A., 1985, *AJ*, 90, 1163
- Band, D., et al. 1993, 413, 281
- Barbier, R. L., et al. 2005, *GCN Circ.* 4397
- Berger, E., et al. 2005, *Nature*, 438, 988
- Berger, E., et al. 2006a, *GCN Circ.* 5952
- Berger, E. et al. 2006b, *ApJ*, 664, 1000
- Blinnikov, S. I., et al. 1984, *SvAL*, 10, 177
- Bloom, J. S., et al. 2008 *GCN Circ.* 7703
- Burrows, D. N., et al. 2006, 2006, *ApJ*, 653, 468
- Burrows, D. N. & Racusin, J. 2007, *astro-ph/0702633*
- Butler, N. R. et al. 2008, *GCN Circ.* 7704
- Campana, S., et al. 2006a, *Nature*, 442, 1008
- Campana, S., et al. 2006b, *A&A*, 454, 113
- Cobb, B. E., et al. 2006, *ApJ*, 651L, 85
- Colgate, S. A., 1968, *CaJPS*, 46, 476
- Copete, A., et al. 2008, *GCN Circ.* 7237
- Covino, S., et al. 2006, *A&A*, 447, L5
- Cucchiara, A., et al. 2007, *GCN* 6665
- Dado, S., Dar, A. & De Rújula, A. 2002, *A&A*, 388, 1079 (DDD2002)
- Dado, S., Dar, A. & De Rújula, A. 2003, *A&A*, 401, 243 (DDD2003)
- Dado, S., Dar, A. & De Rújula, A. 2004, *A&A*, 422, 381 (DDD2004)
- Dado, S., Dar, A., & De Rújula, A. 2007, *ApJ*, 663, 400 (DDD2007a)
- Dado, S., Dar, A., & De Rújula, A. 2007, *arXiv:0706.0880* (DDD2007b)

- Dado, S., Dar, A., & De Rújula, A. 2008a, *ApJ*, 680, 517 (DDD2008a)
- Dado, S., Dar, A., & De Rújula, A. 2008b, *ApJ*, 681, 1408 (DDD2008b)
- Dado, S., Dar, A., & De Rújula, A. 2008c, *ApJ*, 678, 353 (DDD2008c)
- Dado, S., et al. 2008, *ApJ*, 678, 353
- Dar, A. 1998, *ApJ*, 500L, 93
- Dar, A. 1999 *A&AS*, 138, 505
- Dar, A. 2005, *GCN* 2942, 1
- Dar, A. 2006, *ChJAS*, 6, 323
- Dar, A. & De Rújula, A. 2000, [arXiv:astro-ph/0008474](https://arxiv.org/abs/astro-ph/0008474)
- Dar, A. & De Rújula, A. 2004, *Physics Reports*, 405, 203 (DD2004)
- Dar, A. & Plaga, R. 1999, *A&A*, 349, 259
- Della Valle, M., et al. 2003, *A&A*, 406, L33
- Della Valle, M., et al. 2006, *Nature* 444, 1050
- De Rújula, A. 1987, *PhLB*, 193, 514
- De Rújula, A. 2008, [arXiv:0801.0397](https://arxiv.org/abs/0801.0397)
- de Ugarte Postigo, A., et al. 2006, *ApJ*, 648, L83
- Donaghy, T. Q., et al. 2006, [astro-ph/0605570](https://arxiv.org/abs/astro-ph/0605570)
- Eichler, D., et al. 1989, *Nature* 340, 126
- Evans, P. A. 2007, *A&A*, 469, 379
- Fenimore, E. E., et al. 1995, *ApJ*, 448, L101
- Frederiks, D. D., et al. 2007, *Astronomy Letters*, 3, 19
- Fox, D. B., et al. 2005, *Nature*, 437, 845
- Galama, T. J. 1998, *Nature*, 395, 670
- Gal-Yam, A., et al. 2006a, *ApJ*. 639, 331

- Gal-Yam, A., et al. 2006b, *Nature*, 444, 1053
- Garnavich, P., et al. 2003, *ApJ*, 582, 924
- Gehrels, N., et al. 2005, *Nature*, 437, 851
- Gehrels, N. et al. 2006, *Nature*, 444, 1044
- Golenetskii, S., et. al. 2006a, *GCN*, 4881, 1
- Golenetskii, S., et al. 2006b, *GCN*, 5264, 1
- Goodman, J., Dar, A. & Nussinov, S. 1987, *ApJ*, 314, L7
- Graham, J. F., et al. 2008, arXiv:0802.1346
- Grupe, D., et al. 2006, *ApJ*, 653, 462
- Hao, G., et al. 2007, *ApJ*, 659, L99
- Hjorth, J., et al. 2003, *Nature*, 423, 847
- Hjorth, J., et al. 2005a, *Nature*, 437, 859
- Hjorth, J., et al. 2005b, *ApJ*, 630, L117
- Horv ath, I. 2002, *A&A*, 392, 791,
- Hullinger, D., et al. 2005, *GCN Circ.* 4400
- Hurley, K., et al. 2005, *Nature*, 434, 1098
- Hurley, K., et al. 2006, *GCN Circ.* 5702
- Kann, D. A., et al. 2008, arXiv:0804.1959
- Kocevski, D.& Butler, N. 2008, *ApJ*, 680, 531
- Kouveliotou, C., et al. 1993, *ApJ*, 413, L101
- Kumar, P., et al. 2007, *MNRAS*, 376, L57
- La Parola, V., et al. 2006, *A&A*, 454, L753
- Levan, A. J., et al. 2006, *ApJ*, 648, L9
- Liang, E. W., et al. 2007, arXiv:0708.2942

- Malesani, D., et al. 2003, ApJ, 609, L5
- Malesani, D. et al. 2004, ApJ, 609, L5
- Malesani, D., et al. 2005a, GCN Circ. 4407
- Malesani, D., et al. 2005b, GCN Circ. 4412
- Malesani, D., et al. 2006, GCN Circ. 4561
- Malesani, D., et al. 2006c, GCN Circ. 5718
- Malesani, D., et al. 2007, A&A, 473, 77
- Malesani, D., et al. 2008, arXiv:0805.1188
- Mangano, V., et al. 2006, GCN 4565
- Mangano, V., et al. 2007 A&A, 470, 105
- Mao, J., et al. 2008, GCN Report 138.1
- Mazzali, P. A., et al. 2006, ApJ, 645, 1323
- Mazets, E. P., et al. 1981, A&SS, 80, 3
- Melo, V. P., et al. 2005, ApJ, 619, 270
- Meszáros, P. 2006, Rep. Prog. Phys. 69, 2259
- Modjaz, M., et al. 2008, arXiv:0805.2201
- Nakar, E, 2007, Physics Reports, 442, 166
- Norris, J. P., et al. 1984, Nature, 308, 434
- Norris, J. P., et al. 1996, ApJ, 459, 393
- Nousek, J. A., et al. 2006, ApJ, 642, 389
- O’Brien, P. T., et al. 2006, ApJ, 647, 1213
- Ofek, E. O., et al. 2006, ApJ, 652, 507
- Ofek, E. O., et al. 2007, ApJ, 662, 1129
- Paczynski, B. 1986, ApJ, 308, L43

- Pian, E., et al. 2006, *Nature*, 442, 1011
- Piran, T., et al. 2005, *RvMP*, 76, 1143
- Perley, D. A., et al., 2008a, GCN Report 7695
- Perley, D. A., et al., 2008b, GCN Report 7749
- Prochaska, J. X., et al. 2006, *ApJ*, 642, 989
- Racusin, J., et al. 2006a, GCN Circ. 5378
- Racusin, J., et al. 2006b, GCN Circ. 5382
- Racusin, J. L., et al. 2007, GCN Report 70.1
- Ramirez-Ruiz, E. & Fenimore, E. E. 2000, *ApJ*, 539, 12
- Rhoads, J. E. 1997, *ApJ*, 487, L1
- Rhoads, J. E. 1999, *ApJ*, 525, 737
- Roming, P. W. A., et al. 2006, *ApJ*, 651, 985
- Sakamoto, T., et al. 2007, GCN Circ. 7147
- Sato, G., et al. 2006, GCN Circ. 5381
- Schady, P., et al. 2006b, GCN Report 6.1
- Shaviv, N. J. & Dar, A. 1995, *ApJ*, 447, 863
- Shaviv, N. J. & Dar, A. 1995, *MNRAS*, 277, 287
- Soderberg, A. M., et al. 2006a, *ApJ*, 636, 391
- Soderberg, A. M., et al. 2006b, *ApJ*, 638, 930
- Soderberg, A. M., et al. 2006c, *ApJ*, 650, 261
- Stanek, K. Z., et al. 2003, *ApJ*, 591, L17
- Stratta, G., et al. 2007, *A&A*, 474, 823
- Thone, C. C., et al. 2007, arXiv:0708.3448
- Troja, E., et al. 2007, arXiv:0711.3034 (*MNRAS*, in press)

- Ukwatta, T. N., et al. 2008, GCN Report 111.1
- Urata, Y., et al. 2007, ApJ, 668, L95
- Wang, L. & Wheeler, J. C. 1998, ApJ, 504, L87
- Watson, D., et al. 2006, A&A, 454, L123
- Whitmore, B. C. & Schweizer, F. 1995, AJ, 109, 960
- Woosley, S. E., 1993, ApJ, 405, 273
- Wigger, C., et al. 2008, ApJ, 675, 553
- Yonetoku, D., et al. 2007, arXiv:0708.3968
- Zeh, A., Klose, S. & Hartmann, D. H. 2004, ApJ, 609, 952
- Ziaeeepour, H., et al. 2007, GCN Report 74.2

Table 1. Width and photon spectral index of SHBs and their ESEC

SHB	z	$\Gamma(\text{SHB})$	Width[s]	$T_{\text{ESEC}}[\text{s}]$	$\Gamma(\text{ESEC})$
050509B	0.225	1.5 ± 0.4	0.03		
050709	0.161	0.8 ± 0.14	0.22	131	1.98 ± 0.18
050724	0.258	1.38 ± 0.13	0.256	152	2.5 ± 0.2
050813	0.72	1.2 ± 0.5	0.6		
051105A		1.33 ± 0.25	0.028		
051210	> 1.4	1.0 ± 0.33	1.27	40	
051221A	0.546	1.08 ± 0.13	1.4		
051227	0.71 ?	1.09 ± 0.23	0.6	110	
060121	> 1.7	$0.82^{+0.38}_{-0.21}$	1.97		
060313	< 1.1	0.61 ± 0.10	0.7		
060502B	0.287	1.0 ± 0.2	0.09		
060505	0.089	1.3 ± 0.3	4		
060614	0.125	1.57 ± 0.14	5	178	2.13 ± 0.04
060801	1.131	1.3 ± 0.2	0.5		
061006	0.438	0.93 ± 0.07	0.5	130	1.74 ± 0.17
061201	0.111	0.81 ± 0.15	0.8		
061210	0.41	0.79 ± 0.15	0.06	85	1.55 ± 0.28
061217	0.827	0.96 ± 0.28	0.22		
070209		1.02 ± 0.33	0.10		
070406		0.9 ± 0.4	0.7		
070429B	0.902	1.53 ± 0.40	0.5		
070714B	0.922	0.86 ± 0.10	3	65	1.36 ± 0.19
070724A	0.457	1.81 ± 0.33	0.40		
070729		1.08 ± 0.36	0.9		
070809	0.2187	1.69 ± 0.22	1.3		
070810B		1.44 ± 0.37	0.08		
071112B		0.69 ± 0.34	0.30		
071227	0.383	0.99 ± 0.22	1.8	100	
080123		$1.22^{+0.21}_{-0.52}$	0.40	115	$2.15 + 0.54$

Based on data cited in Kann et al. 2008 and from
http://gcn.gsfc.nasa.gov/gcn3_archive.html.

Table 2. CB model parameters of SHBs’ afterglows

SHB	$t_1[s]$	$\Delta t_1[s]$	$t_b[s]$	$\theta \gamma_0$	p^a	$t_f[s]^b$	$\Delta t_f[s]^b$
050709	—	—	46733	0.716	(2.2)	—	—
050724	16.2	58.9	2170	0.327	1.56	3138	37244
051210	0	92.3	—	—	—	—	—
051221A	0	63.9	11591	1.15	2.2	—	—
051227	85.0	24.0	1260	1.026	2.33	—	—
060121	—	—	6754	1.031	2.2	—	—
060313	175.4	246.0	1442	1.025	2.2	2.1	138
060801	0	104.5	—	—	—	—	—
061006	0.17	89.9	8561	0.778	(2.2)	—	—
070714B	40.7	107.8	1672	1.12	(2.2)	30.2	49.2
070724A	87.8	108.9	1531	1.483	(2.2)	58.9	48.8
071227	89.2	31.4	3093	1.164	(2.2)	0	8.86
080123	150.5	24.9	3501	0.865	(2.2)	0	28.9
080503	20.1	47.1	218946	(1.00)	(2.2)	—	—
060614	16.8	42.9	3829	3.079	2.14	—	—

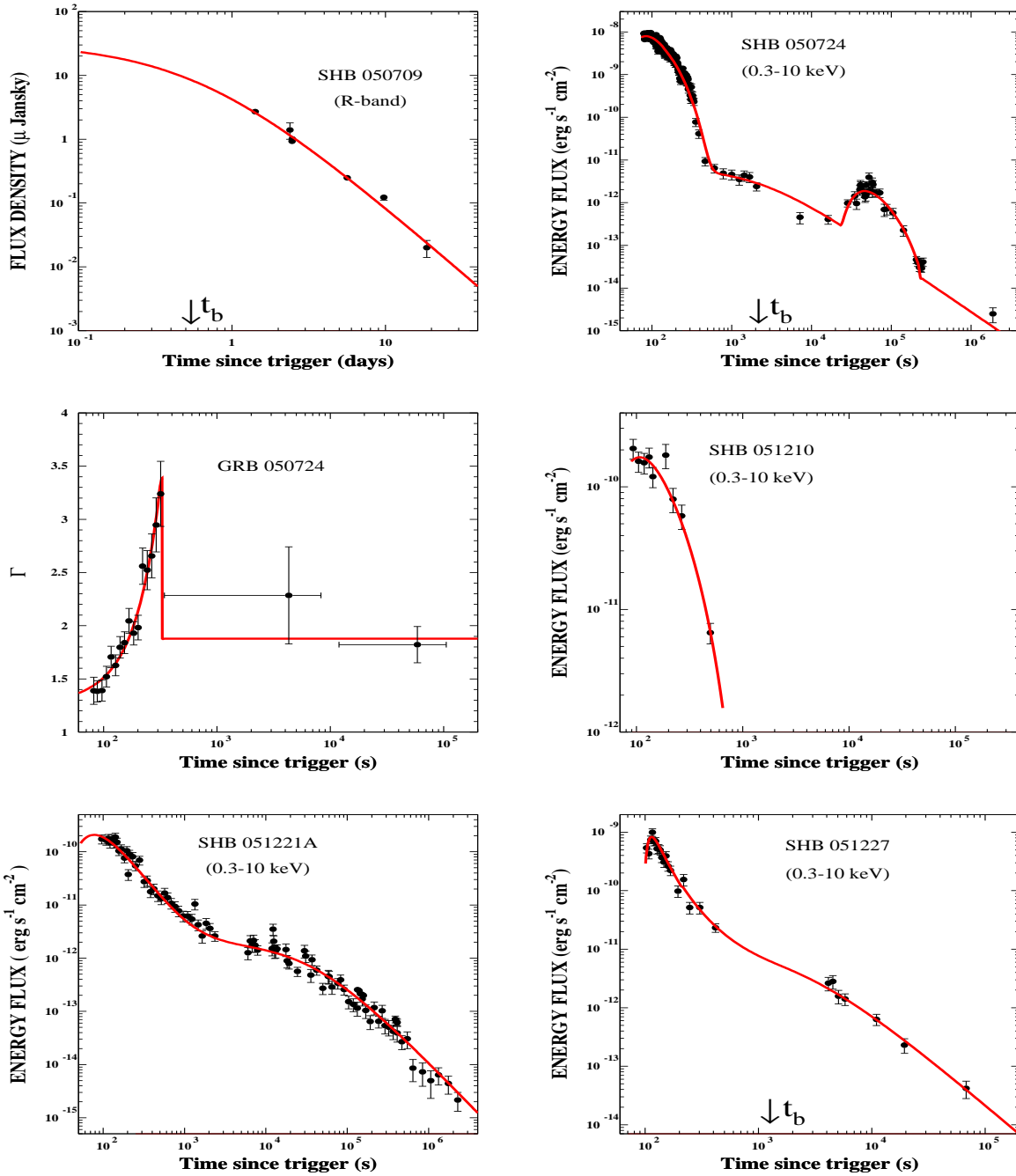


Fig. 1.— Comparisons between SHB observations and CB model predictions for **Top left (a)**: The R-band light curve of SHB 050724 (data from Watson et al. 2006). **Top right (b)**: The XRT/Chandra light curve of SHB 050724 **Middle left (c)**: The evolution of the photon spectral index of GRB 050724 (data from Zhang et al. 2007). **Middle right (d)**: The XRT light curve of SHB 051210. **Bottom left (e)**: The XRT light curve of SHB 051221A. **Bottom right (f)**: The XRT light curve of SHB 051227.

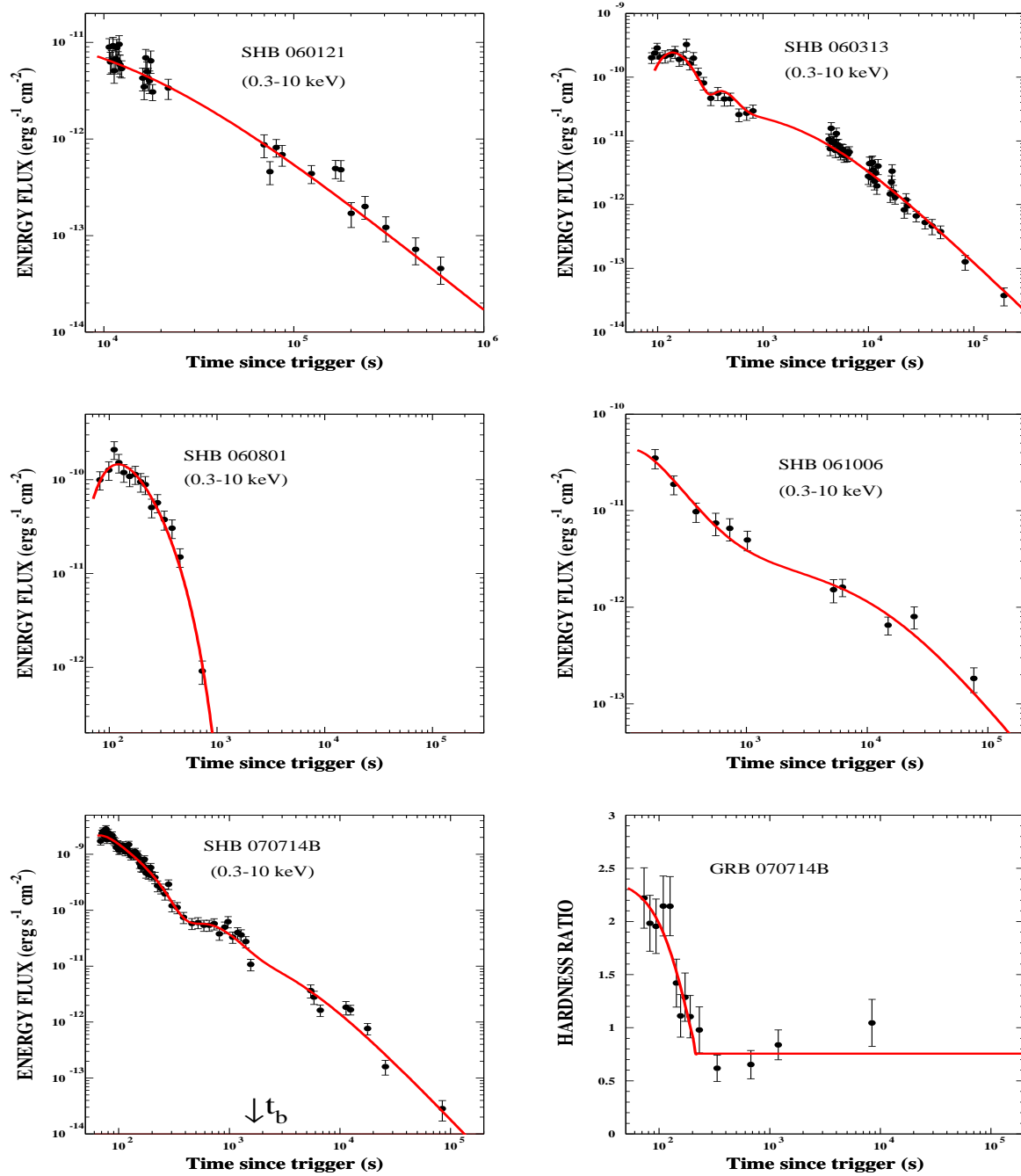


Fig. 2.— Comparisons between SWIFT XRT observations of SHBs (Evans et al. 2007) and the CB model predictions. **Top left (a):** The light curve of SHB 060121. **Top right (b):** The light curve of SHB GRB 060313. **Middle left (c):** The light curve of SHB 060801. **Middle right (d):** The light curve of SHB 061006. **Bottom left (e):** The light curve of SHB 070714b **Bottom right (f):** The hardness ratio of 070714b.

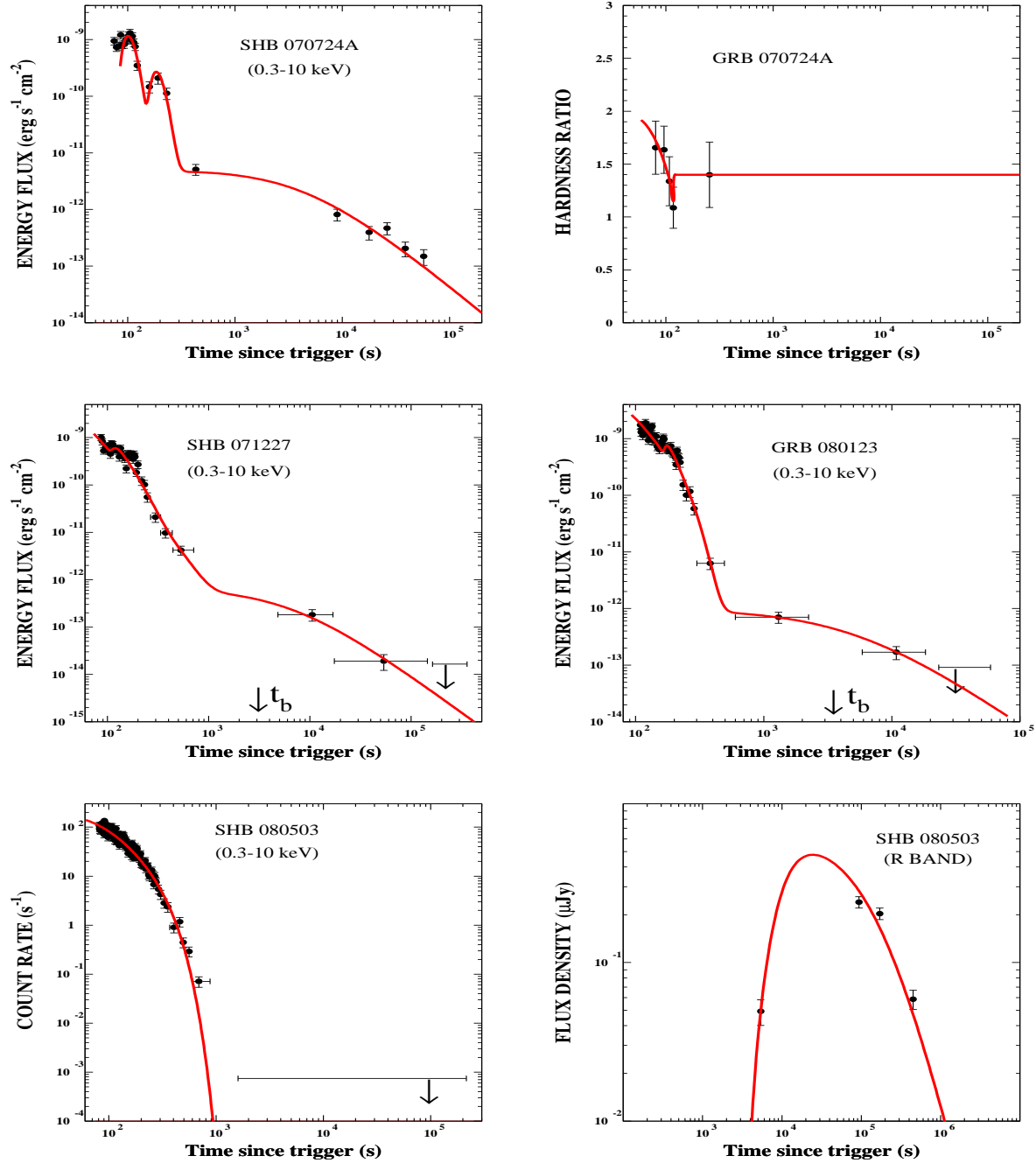


Fig. 3.— Comparisons between observations of SHBs and CB model predictions. **Top left (a):** The XRT light curve of SHB 070724A. **Top right (b):** The hardness ratio of SHB 070724A. **Middle left (c):** The XRT light curve of SHB 071227. **Middle right (d):** The XRT light curve of SHB 080123. **Bottom left(a):** The XRT light curve of SHB 080503. **Bottom right (b):** The R-band light curve of SHB 080503.

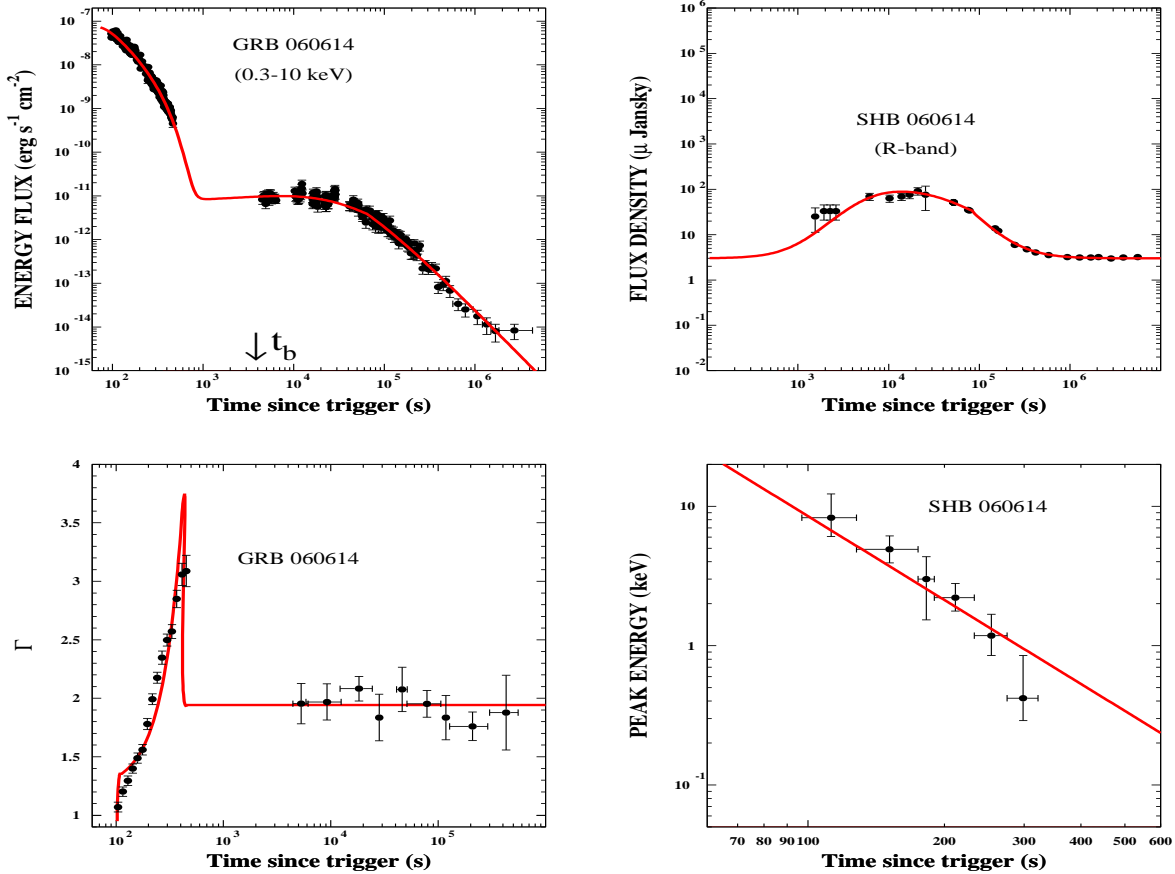


Fig. 4.— Comparisons between observations and CB model predictions. **Top left (a):** The X-ray light curve of SHB 060614 (Evans et al. 2007). **Top right (b):** The R-Band light curve of SHB 060614 (Della Valle et al. 2006). **Middle left (c):** The photon spectral index light curve of SHB 060614 (Zhang et al. 2007). **Middle right (d):** The peak energy evolution during the fast decay of the ESEC in SHB 061614

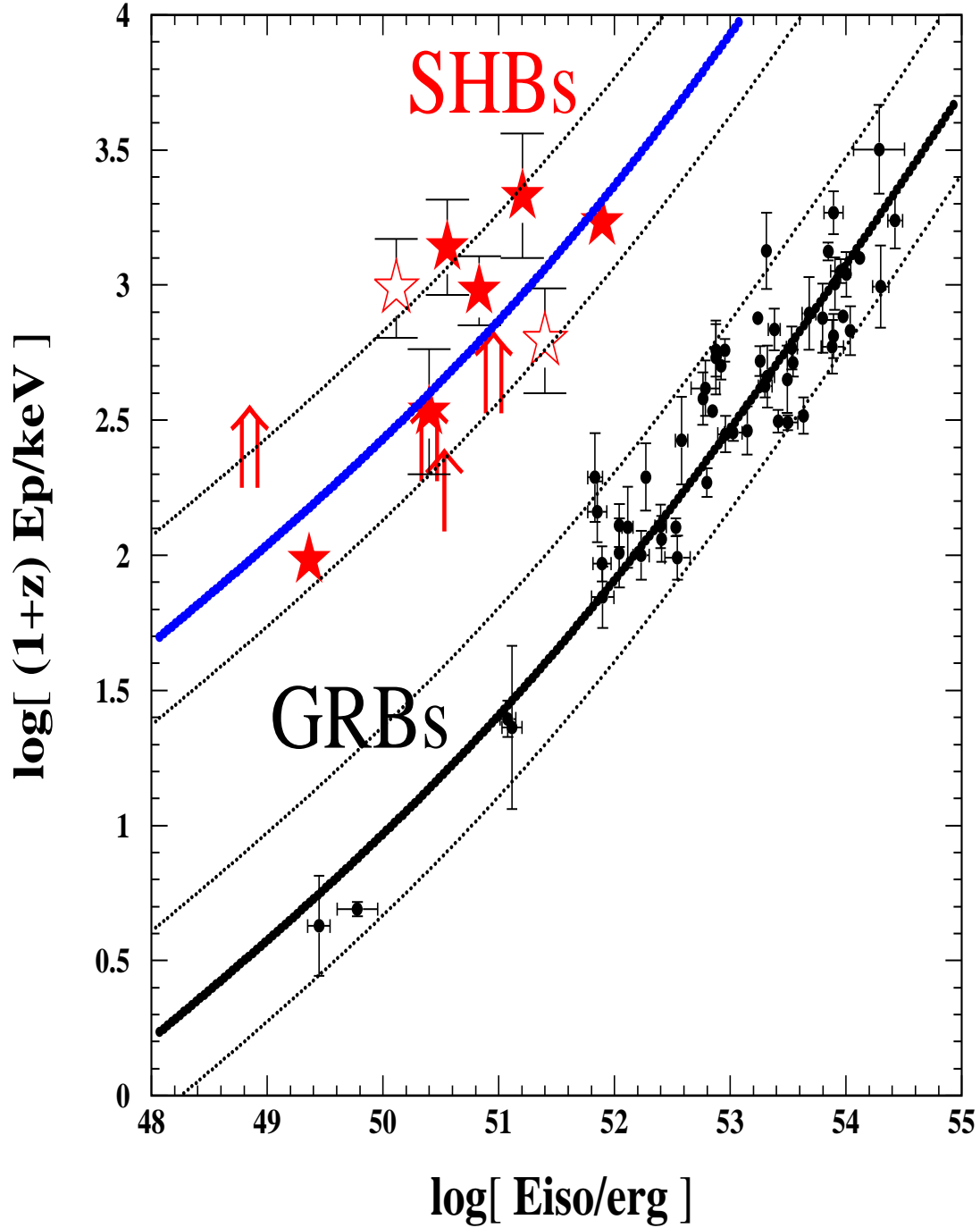


Fig. 5.— Comparison between the observed correlation $[E_p, E_{iso}]$ in LGRBs and SHBs and the CB model expectations for LGRBs (DDD2007a) and SHBs as given by Eq. (22).